Reconstructing the Ischemic Cerebrum by Transplanted Human Neurons

Zhifu Wang[1 †*], Danyi Zheng[1 †], Phil Jun Kang[2], Fei Ye[1], Su-Chun Zhang[1,2,3 *]

[1]Program in Neuroscience and Behavioral Disorders, Duke-NUS Medical School, Singapore

[2]Center for Neurologic Diseases, Sanford Burnham Prebys Medical Discovery Institute, La Jolla, CA, USA

[3]Waisman Center, University of Wisconsin-Madison, Madison, WI, USA

[†]These authors contributed equally

[*]Correspondence: wang.zhifu@duke-nus.edu.sg, suchunz@sbpdiscovery.org

Highlights

Human ESC-derived cortical neurons reconstitute the ischemic motor cortex

Functionally repaired corticospinal tract restores animal behaviours

Transplanted cortical neurons exhibit subtype-specific projection and integration

Grafted neuronal subtypes carry unique transcriptional coding for axonal projection

Summary

Neural transplantation holds the potential to repair damaged neural circuits in neurological diseases. However, it remains unknown how the grafted neurons project axons to and make functional connections with the appropriate targets to repair the damaged circuit at the adult stage. Here we report that human cortical progenitors, transplanted into the ischemic mouse motor cortex, matured and integrated into cortical and subcortical neural circuits including the corticospinal tract. Neuronal tracing

combined with single-nuclei RNA sequencing revealed the close relationship between the transcription profiles of a cortical neuronal subtype, especially those of axon guidance and synapse assembly, with the specific target projection and synapse organization. Machine learning-based regression further identified the transcriptional codes for the targeted projection and circuit integration to reconstruct the damaged circuits. Our finding opens a promising strategy for treating neurological diseases through promoting regeneration and neural transplantation.

Introduction

The human brain has a limited regenerative capacity. Transplantation of neural progenitor cells (NPCs) offers a promising approach to replace the lost neurons and reconnect the damaged circuits. Indeed, transplantation of NPCs derived from pluripotent stem cells, including human embryonic stem cells (hESCs) or induced pluripotent stem cells (hiPSCs), is now in clinical trials for Parkinson's disease (PD), epilepsy, and age-related macular degeneration. However, how the grafted neurons find and make functional connections with their targets in the mature injured brain remains unclear. This makes neural transplantation therapy less predictable, especially for diseases of the cerebral cortex that affect diverse neuronal subtypes and multiple neural circuits including the long-distance corticospinal tract (CST).

Cortical neurons or organoids transplanted into the postnatal brain exhibit low efficiency in extending axons from the neocortex to the brainstem[1], with even fewer projections observed when grafted into the brains of adult animals following traumatic brain injury or stroke[2,3]. Meanwhile, the injury leaves an open cavity surrounded by glial scars, resulting in a hostile microenvironment that severely limits the survival and integration of transplanted neurons, preventing effective structural repair and reconstruction of the damaged neural circuitry. Single cell profiling of retrogradely labelled neurons revealed the self-organized process during development based on the association between the transcriptome of cortical neuronal subtypes and their projection targets[4-6]. However, the injured brain environment at adult stage differs significantly

from the developing brain in both structure and molecular composition, and circuit integration relies on a complex combination of guidance molecules[7]. Substantial numbers of graft-derived axons are often observed in stochastic, unrelated brain regions. Even the neurons originating from the visual cortex, transplanted into the visual cortex, project to the agranular insula, striatum, amygdala, and superior colliculus[8-10], only partly corresponding to the host neural circuits. On the other hand, hESC-derived midbrain dopaminergic (mDA) neurons, transplanted into the substantia nigra (SN), primarily grow axons along the medial forebrain bundle (MFB) to innervate the striatum[11,12], whereas cortical neurons transplanted into the SN project to the prefrontal cortex[11]. These phenomena suggest that the organization principle of the projection and connectivity in the damaged adult brain is different from the self-organizing processes observed during brain development[13]. Hence, identifying the basic principle of pathfinding and circuit integration by grafted neurons in the mature brain will enable us to develop not only a predictable as well as safe and effective cell transplantation therapy but also regenerative therapy for brain disorders.

We reconstructed subcortical neuronal circuits, including the CST, in the ischemic stroke brain by transplanting subtype-specific deep-layer cortical neurons. These specific cortical neurons facilitated more efficient establishment of targeted projections and were sufficient to reconstruct long-distance neural circuits without overgrowth. This finding suggests a potential link between neuronal projection directions and neuronal subtype identity. One way to determine whether the projection and connectivity of transplanted neurons follow a specific pattern is to couple projection-defined subtypes and transcriptome-defined subtypes. We approached to this strategy by transplanting hESC-derived cortical neurons (with multiple subtypes) into the ischemic motor cortex of adult mice and identifying the transcription profiles of cortical neuron subtypes that project to and connect with specific post-synaptic targets following retrograde and antegrade tracing. The transplanted cortical neurons showed subtype-specific projection and integration. The subtypes of hPSC-derived cortical neurons, transplanted in the adult brain, possess distinct combinations of axon guidance

and synaptic assembly molecules that are similar to but distinguishable from those required in endogenous human neurons. We further identified the transcriptional codes for specific projection and circuit integration in the mature brain with machine learning. These findings highlight the necessity of developing appropriate neural types for integration into target neural circuits in the injured brain by neural transplantation at adult stage.

Results

Transplanted human cortical neurons project to specific brain regions

The stroke cavity presents a hostile environment for transplanted cells; hence, grafting is typically performed in adjacent healthy brain regions instead[3,14-16], leaving the injured cortex open and unrepaired. We previously developed a cocktail that supports the survival of neural cells transplanted into the ischemic cavity[17]. To reconstitute the ischemic cortex and restore damaged circuits, we first differentiated hESCs into cortical NPCs for transplantation (Figure 1A). The cortical NPCs at day-35 contained over 70% progenitors expressing both CTIP2 and FEZF2 (markers of layer 5 pyramidal neurons) with less than 20% expressing layer-6 marker TBR1 (Figures 1B and S1A-S1B). These NPCs were transplanted into the lesion cavity of ischemic stroke models, induced by photothrombosis in the motor cortex of 12-week-old immunodeficient mice. In total, we successfully performed cortical neuron transplants in 83 mice (Supplementary Table 1). Twelve months post transplantation, the graft filled the stroke cavity with no overgrowth (Figures 1C and S1C).

Immunohistochemical analysis showed that 90% of transplanted cells expressed the neuronal marker NeuN (Figures 1D and 1E), indicating differentiation into neurons. About 63% of grafted cells were CTIP2^{+}/ FEZF2^{+}/ TBR1^{-} neurons (Figures 1F and 1G), consistent with the pre-transplantation cell population, suggesting that these cortical NPCs were cell fate-committed before transplantation. Single-nucleus RNA sequencing (snRNA-seq) revealed that the grafted human cells were predominantly

deep layer neurons, with only a small fraction of upper layer and GABAergic neurons (Figures S1D-1H). Less than 10% of transplanted cells differentiated into astrocytes ($SOX9^+$), and none into microglia and oligodendrocytes (Figures S1I-S1K). At this stage, no KI67-expressing human cells were detected (Figure S1L). Thus, transplanted human NPCs survived and differentiated into deep-layer cortical neurons, with stable proportions of $CTIP2^+/FEZF2^+$ cells pre- and post-transplantation. We also observed that graft-derived axons ($hNCAM^+$) were enveloped by MBP^+ cells (Figure S2A). Since no human cells become oligodendrocytes, indicated by histology (Figure S2B) and snRNA-seq (above), the MBP^+ cells are originated from mouse oligodendrocytes. Additionally, mouse endothelial cells ($Laminin^+$) infiltrated the graft (Figure S2C), enabling blood vessels to support the grafts in a long term.

We evaluated the extension of graft-derived axons by human-specific hNCAM staining (Figure 1H), which revealed extensive axonal projections from the graft to cortical and subcortical brain regions. Semi-quantification of $hNCAM^+$ axonal density in the whole brain revealed that the graft-derived axons were not only present along CST, but also in the somatosensory cortex (S1), thalamus, superior colliculus, medial vestibular nucleus, and SC (Figures S3A-S3E and S3H). In contrast, only a small number of axons followed the corpus callosum (cc) to reach the contralateral hemisphere (Figures S3F and S3H). Therefore, we focused our analysis on the projection and connectivity in the ipsilateral hemisphere. Robust projections were observed along the host CST from the striatum to the brainstem, as revealed in sagittal sections (Figure 1I). To clearly visualize graft-derived axons in the pyramidal tract, we performed tissue clearing and 3D reconstruction for $mCherry^+$ transplanted neurons in the brain by light-sheet microscopy (Figure 1J). Fascicular $mCherry^+$ axons extended through the midbrain along the pyramidal tract, decussated at the medulla, and continued into the spinal cord (Figures 1J-1L and S3G). Such a projection pattern of transplanted neurons ($CTIP2^+$/ $FEZF2^+$/ $TBR1^-$) resembles that of endogenous corticospinal neurons.

Transplanted neurons exhibit selectivity in forming synapses with host neurons in the subcortical regions

Functional restoration depends on integration of transplanted neurons into the existing circuits. To evaluate the global post-synaptic connectivity of transplanted neurons in the adult brain and spinal cord, we developed an ESC line that expresses the anterograde trans-synaptic protein mWGA-mCherry (mWmC), a mono-synaptic tracer[18], driven by the *synapsin1* promoter (Figure 2A). In vitro, the mWmC was only detected in neurons (NeuN+) but not in non-neural cells (Figure S4A). Following transplantation, we detected mWmC signals in the host neurons, suggesting that transplanted neurons formed synaptic connections with downstream host neurons (Figure 2B). A substantial number of mWmC-positive host neurons were observed in the S1, striatum, thalamus, subthalamic nucleus (STN), superior colliculus (SuC), pontine gray (Pon G) (Figures 2C-2G). In contrast, despite extensive graft-derived axons, there were few mWmC-labelled cells observed in the substantia nigra (Figure 2G). These results indicate that specific transplanted neurons make connections with neurons in specific target brain regions until their axons reach the targets rather than form stochastic connections with nearby host neurons based on proximity alone.

We next mapped the connections of graft-derived axons, showing that the transplanted neurons projected to and established synaptic connectivity in motor-related brain areas including S1, striatum, thalamus, STN, SuC, and Pon G (Figure 2H and 2I). This is strikingly similar to the endogenous targets of the motor cortex when we mapped the post-synaptic connectivity by AAV-mWmC injection into the motor cortex (Figure S4B). Notably, mWmC-positive cells were detected in the SC, primarily on the contralateral side (Figure 2J), implying that the transplanted neurons are integrated in the corticospinal circuits. Remarkably, these transplanted human neurons connected with lower motor neurons ($ChAT^{+}$) in the ventral horn of the spinal cord (Figure 2J), whereas rodent upper motor neurons usually form indirect connections with lower motor neurons through interneurons rather than direct connection[19-21].

At the cellular level, our immunohistochemistry results showed that the transplanted neurons established connections with CTIP2+ spiny GABAergic projection neurons in the striatum (Figure S5A), (vGLUT1^{+}) glutamatergic and (GAD67^{+}) GABAergic neurons in the thalamus, and glutamatergic neurons in the STN, as indicated by the mCherry signal in those cells (Figures S5B, S5C, and S5F). Meanwhile, mWmC was not detected in dopaminergic neurons in the substantia nigra (SN) (Figure S5D). The grafted neurons formed post-synaptic connections with interneurons in the SC (Figures S5E and S5F).

Transplanted cortical neurons make functional connections with host neurons

To test if the connections between transplanted neurons and host neurons are functional, we generated a DREADD/mWmC hESC line which expresses the excitatory hM3Dq receptor regulated by Deschloroclozapine (DCZ) and the trans-synaptic tracer mWmC (Figures 3A and S6A). This strategy allows us to simultaneously assess trans-synaptic connections using mWmC labelling and functional synaptic connectivity via DREADD activation. Administration of DCZ (0.05mg/kg) significantly increased the expression of the activity-dependent protein FOS in transplanted neurons, indicating that DCZ treatment activated the transplanted DREADD/mWmC neurons (Figure 3B). Immunohistochemical co-staining of FOS and WGA showed that following DCZ activation of the transplanted neurons, the proportion of synaptically connected host neurons (WGA^{+}) expressing FOS also significantly increased, while there was no significant change in host neurons (WGA^{-}) without synaptic connections with the graft (Figure 3B and 3C). These data indicate that transplanted neurons formed synaptic connections with host neurons and influenced their activity.

To investigate whether the neural circuits regulated by transplanted neurons restore motor function in the stroke mice, we used NPCs from an inhibitory hM4Di DREADD hESC line as donors (Figure 3D and S6B-S6C). Gait analysis by Treadscan showed that cell transplantation improved motor function in stroke mice (Figures 3E and 3F). However, after DCZ administration to inhibit the transplanted neurons, the motor

functions significantly declined, indicated by reduced time and frequency of the front left paws (contralateral side) touching the treadmill belt (Figures 3F and 3G). Footprint analysis of the front left paw (FL) revealed that inhibiting the transplanted neurons led to a recurrence of motor dysfunction in the previously recovered left limb (Figures 3H and 3I). Upon grafted neuron inhibition via hM4Di activation, there was a significant increase in the swing time of the left paw, while no notable changes were observed in the right paw (Figure 3J). Meanwhile, the mice stayed close to the contralateral wall after DCZ treatment (Figure 3K). These data suggest that the transplanted neurons form functional connections with the host neurons, and the neural circuits repaired by transplanted cortical neurons underlie the motor function restoration.

Projection of transplanted cortical neurons is subtype-specific in the ischemic brain

Transplanted cortical neurons extended axons to multiple targets, prompting a critical question of how the axonal targeting is regulated in the injured adult brain. To address this, we combined multiple retrograde tracing with snRNA sequencing (MRT-seq)[5] to reveal the transcriptional profiles of grafted neurons projecting to specific regions. Four retrograde AAVs (GFP^+), each carrying a unique barcode, were injected into the primary somatosensory cortex (S1), striatum, thalamus, and medulla (MY) five weeks prior to graft dissection for snRNA-seq (Figure 4A). The retro-AAV broadly labelled the L5 and L6 host cortical neurons (Figure S7A), as expected. The transplanted neurons, labelled by GFP (Figure 4B) and collected from three animals for snRNA-seq (Figures S7B and S7C). Strikingly, the retrogradely labelled grafted neurons formed distinct clusters (Figure 4C), indicating that projection-defined neuronal groups correspond to specific transcriptional subtypes. Cortical projection neurons are commonly classified into four subtypes: extratelencephalic (ET), intratelencephalic (IT), corticothalamic (CT), near-projecting (NP) neurons[22], although snRNA-seq revealed at least 100 putative cortical neuronal subclasses[23]. Alignment with a public dataset of adult human M1 cortex (Figures S7D and S7E) revealed that retrogradely

labelled cells partially correspond to four neuronal subtypes: L5 ET, L5 IT, L6 CT, and L5/6 NP (Figures 4C and 4D). Therefore, we named the grafted cortical neurons as grafted L5 intratelencephalic (G-L5 IT, striatum-projecting), grafted L6 CT (G-L6 CT), grafted L5 extratelencephalic (G-L5 ET, medulla-projecting), and grafted L5/6 near-projecting (G-L5/6 NP) neurons.

To identify the transcription profiles of G-L5 ET neurons projecting to the SC, we injected retrograde AAV with GFP in the contralateral SC and retro-AAV with RFP in the ipsilateral SC, both at the C7-T1 segments (Figures S7F-S7I). The host neurons labelled by AAV in the intact cortex were located in L5 (Figure S7H). 97% of retrogradely labelled grafted neurons projected to the contralateral SC (GFP^+) whereas only 3% to the ipsilateral side (RFP^+), as indicated by snRNA-seq (Figure 4E). Over 86% of all labelled cells belonged to the same neuronal cluster, and it shared a similar transcriptome with G-L5 ET (Figure 4F), including HCN1, KCNH1, BCL11B, SGCZ, GRIK2, and CNTN3. In particular, HCN1 channel-dependent membrane properties can distinguish L5 ET (human Betz cells) from L5 IT neurons[24]. Betz cells are characterized by low input resistance and distinct peak resonance, reflecting their large size and the high expression of genes associated with the HCN channel[24,25]. The projection pattern of G-L5 ET neurons in the SC is also similar to that of human Betz cells (Figure S7J). To explain the relatively human-specific connections in rodents, we analyzed the DEGs of synaptic assembly between human and mouse corticospinal neurons. A specific combination of synaptic assembly genes, including ROBO2, NRCAM, and L1CAM, was significantly higher in the G-L5 ET neurons compared to mouse corticospinal neurons (Figure S7K). ROBO2, NRCAM, and L1CAM are critical receptors on the growth cone to connect to lower motor neurons[26-28]. They also play a vital role in commissural neurons to form the decussation of the pyramids.

These data indicate substantial transcriptomic differences among the four projection defined subtypes of transplanted neurons. To investigate how transcriptomic differences influence the projection patterns of these neurons in the adult brain, we analyzed the DEGs among transplanted neurons with distinct projection targets. Gene

ontology (GO) analysis of DEGs in G-L5 ET, G-L5 IT, G-L6 CT, and G-L5/6 NP neurons revealed that the top GO terms of biological processes were associated with axon guidance and synapse organization/transmission (Figures 4G and S7L-S7N). Among the four projection-defined subtypes, each expressed distinct combinations of canonical axon guidance genes, such as ROBO1, ROBO2, SLIT1, SLIT3, and EPHA3 (Figure 4H). These results highlight the transcriptomic predominance of specific genes related to axonal projection, explaining why transplanted neurons of one specific transcriptomic subtype mainly project to the same brain region.

The projection pattern is regulated by transcription factors

We then ask whether modifying neuronal subtypes or their corresponding transcriptional codes through transcription factors can alter their projection pattern in the disease model. Ctip2 is an essential transcriptional factor in L5 cortical neurons[29,30]. We generated a CTIP2 knockdown (CTIP2-kd) hESC line and transplanted CTIP2-kd NPCs into the ischemic cortex (Figure 5A). Interestingly, the axons of CTIP2-kd neurons primarily projected to the amygdala (Amy) through the stria terminalis (ST) in the ipsilateral hemisphere (Figures 5B and 5C), with minimal projections to the subcortical regions (Figures 5B and S8A-S8C). Quantification of projections showed that the projection pattern of CTIP2-kd neurons was significantly different from that of wild-type neurons with more to hippocampus, basolateral amygdaloid nucleus (BLA), and basomedial amygdaloid nucleus (BMA) but less to subcortical regions (Figures 5D and 5E). Furthermore, robust axons from transplanted CTIP2-kd neurons crossed to the contralateral cortex through the corpus callosum (cc), which is rarely observed in wild-type ESC-derived neurons (Figure 5F). In germline Ctip2-deficiency mice, although the L5 neurons lack robust axons along the CST, they still project to subcortical regions and do not cross to the contralateral hemisphere[29]. The distinct projection patterns from grafted CTIP2-kd grafted neurons indicates the differences in axon guidance between the self-organizing and the mature brain environment.

To reveal how CTIP2-kd alters axonal pathfinding, we integrated the snRNA profiling of control and CTIP2-kd cells and found that while their transcriptome distance is close, 76% of CTIP2-kd cells were not identified as any wild-type grafted neuron subtype (Figures 5G and S8D), indicating modified neuronal subtypes. The CTIP2-kd neurons also lack the markers of wild-type grafted neurons, such as LDB2 and FOXP1 (Figure 5H). The top-10 GO terms of biological process are linked to axon guidance and connectivity (Figure 5I). Among them, 61.5% of DEGs are related to axon projection (Figure S8E). In particular, the RNA levels of the axonal guidance molecules normally expressed in L5 ET neurons, such as ROBO2 and SLIT3, were downregulated whereas EFNB1, EFNB2, NRP2 were upregulated after knocking down CTIP2 (Figure 5H). ROBO2 and SLIT3 are required for forming the subcortical projection while EFNB1, EFNB2, and NRP2 play critical roles in guiding axons toward the amygdala and the contralateral hemisphere, which may explain the altered axonal trajectory. Hence, modification of the transcriptome by altering a single transcription factor such as CTIP2 changes the axonal trajectory, highlighting the requirement of a special code for the same neuronal type to navigate in the mature brain.

Grafted neuronal subtypes carry unique transcriptional codes for axonal projection

The above analysis revealed the match between the transplanted cortical neuronal subtypes and the expected projection targets, raising the intriguing question of how hPSC-derived neurons navigate and establish connectivity within the disorganized environment of the injured brain, in contrast to the self-organizing processes during development. We first evaluated the maturation state of the grafted neurons by comparing with human cortical neurons at different stages (Figure 6A)[24,31]. The clusters of grafted neurons predominantly overlap with adult deep-layer cortical neuronal types (Figure S9A), while fewer clusters overlap with postnatal neurons (Figure S9B). The similarity was further validated by pseudotime analysis (Figures S9C-S9F). Our data indicate that the four subtypes of 12-month grafted human neurons transcriptomically

resemble the corresponding subtypes of adult human cortical neurons in the M1 (Figure 3A). Both G-L5 ET and H-L5 ET neurons possess significantly higher expression levels of ROBO2, PTPRM, and SEMA3D (Figures 6A and S9G), which likely facilitate the formation and maintenance of corticospinal connections with spinal motor neurons[24,32]. Interestingly, several axon guidance molecules, including DRAXIN, UNC5C, FLRT2, and NEO1, are more highly expressed in grafted corticospinal neurons compared to endogenous human neurons (Figure S9G). These molecules are associated with axonal repulsion, suggesting that stronger repulsion-mediated pruning may be essential for directing axons along correct trajectories in the adult brain, which is also observed in L5 IT, L6 CT, and L5/6 NP neurons (Figure 6A). This may help explain why transplanted neurons, although closely mimicking endogenous neurons in function, often fail to extend their axons to appropriate target regions.

We next sought to identify the transcriptional code for each of the subtypes that establish projections to the intended target regions (on-target), as opposed to those that merely exhibit transcriptomic profiles resembling their cortical counterparts without appropriate targeting (off-target), by comparing the transcriptomic differences between projection-defined subtypes and their human counterparts. A set of 100 genes was calculated from all genes using the "SelectKBest" method with the "f_classif" statistical test to define grafted neurons in each subtype and further refined using L1-regularized logistic regression and cross-validated by Bayesian Additive regression trees to obtain a code with minimal numbers of genes (Figure 6B). Although the gene expression profiles of one specific neuronal subtype are largely overlapping, our results demonstrate that differential expression of several selected genes is sufficient to distinguish on-target neurons from off-target neurons, serving as a form of transcriptional codes for grafted neurons (Figures 6C and 6D). Across the four neuronal subtypes, these gene combinations exhibit distinct variations, suggesting the subtype specificity. Notably, most of these genes are implicated in axon guidance and synapse organization, including GPHN, KALRN, PTPRD, DSCAM, NRXN1, NRXN3, GRIA2,

ANK2, NEGR1, NRG3, LRRTM4, LRRC7, MEG3, CADM2, DLG2, and CNTNAP2 (Figure 6C).

To validate our formulation, we analyzed the neuronal subtypes in the cortical organoids transplanted into the mouse S1 cortex[13] by integrating the snRNA-seq reference dataset (Figure 6E). According to our transcriptional code-based identification, the neurons in the transplanted cortical organoid comprised 0.34% G-L5 ET, 0.20% G-L6 CT, 23.66% G-L5/6 NP, and 14.36% G-L5 IT on-target neurons (Figure 6F). Indeed, the transplanted (organoid) neurons project predominantly to the ipsilateral cortical and striatal regions but rarely to the pyramidal tract and the ventrolateral/ventromedial thalamic nucleus [13], supporting the accuracy of our model. Our findings show the critical role of specific axon guidance profiles in defining the neuronal subtypes. These transcriptomes, while similar to those of the corresponding adult human neuronal subtypes, exhibit changes in combination and/or expression levels, serving as transcriptional codes for the grafted neurons to find their targets in the adult CNS.

Discussion

Defining if and how the transplanted neurons find and make functional connections with their targets in the adult brain will enable us to develop effective strategies for and predict the outcome of cell therapy. We established the correspondences between projection targets and transplanted neuronal subtypes and identified the transcriptional code for specific axonal guidance and synapse assembly in the mature brain with machine learning-based regression analysis. These transcriptional codes associate transplanted neuronal identity with their projection patterns. This is further supported by findings that changes in neuronal identity induced by transcription factors such as CTIP2 result in profound alterations in axonal projections and target recognition, suggesting that the projection directions of transplanted neurons in the mature brain can be modulated through transcription factor regulation. The circuits reconnected by the

transplanted human cortical neurons are specific and functional, as indicated by the mono-synaptic antegrade tracing and activity-dependent FOS expression in the target neurons, corresponding to motor behavioural recovery of the stroke mice. These transcriptome profiles serve as tags to identify the complex guidance combinations, setting the foundation for developing specific cell types for circuit repair.

It has been demonstrated that transplanted neurons form functional connections with host neurons, contributing to the therapeutic effects in animal models of neurological diseases[13,33-36]. The premise for choosing specific types of neuronal cells for transplantation is based on the information we have learned in developing animal models, i.e., a developing neuron finding its targets is largely determined by its specific transcriptiome[6,37-39]. However, the environment of the brain undergoes substantial modification after maturation, which alters the organization patterns of projections and connectivity. Hence, the axonal projection of grafted neurons to their long-distance targets is usually insufficient[2,3], or establishes inappropriate connections[40]. It is thus desirable to identify the intrinsic properties or transcriptional codes of the transplantable neuronal cells to achieve high-fidelity circuit integration in the adult brain. Hence, we identified the specific combinations of axonal guidance and synapse organization gene profiles or codes for each cortical neuronal subtype. Notably, transplanted neurons exhibited a pronounced upregulation of repulsive guidance cues compared to endogenous neurons[24]. This differential expression pattern suggests the special balance between attractive and repulsive guidance signals required for axonal navigation in the adult brain. The drastic change in projection patterns by the grafted cells with CTIP2-kd highlights the regulatable properties of the grafted neurons in pathfinding and circuit integration even in the adult brain. Indeed, the corticospinal neuronal subtype in our transplanted cells project axons via the pyramidal tract, cross over to the contralateral side at the medulla level, and reconnect with the spinal motor neurons, which corresponds to the motor behavioural recovery of the stroke mice. A striking feature of such connections is direct synaptic connection between the human cortical motor neurons and the mouse spinal motor neurons, a property in primates, besides indirect

synapses through interneurons, a characteristic in rodents. Such a phenomenon again highlights the critical role of the specific transcriptional code of the grafted neurons in circuit integration. Thus, the transcriptome of the transplanted cortical neuron subtypes may serve as identity tags to predict their projections and connectivity, providing a guideline for selecting appropriate neuronal cell types for targeted circuit reconstruction.

The high-fidelity circuit reconstruction through transplanted neurons is influenced by numerous factors. Our study revealed the roles of transcriptional codes of the major cortical neuronal subtypes in pathfinding and synaptic assembly in the mature brain. Analysis of additional neuronal types in other model systems will help determine if it is a general principle. The similarity to as well as the difference from their endogenous counterparts suggests the potential impact of the environmental signals in modulating the transcription of the grafted cells, which warrants investigation.

Methods

All experiments were carried out according to the protocol approved by the Institutional Animal Care and Use Committee at Duke-NUS Medical School.

Cell Culture

Human embryonic stem cells (hESCs) were cultured in a feeder-free mTeSR PLUS medium (STEMCELL, CAT#: 100-0276) with 1 × mTeSR supplement, 1 × Non-Essential Amino Acids (NEAA; Gibco, CAT#: 11140050) and 1 × GlutaMAX Supplement (Gibco, CAT#: 35050061) in a Matrigel (Corning, CAT#: VMA00048) coated 6-well plate. hESCs were fed daily and passaged every three days.

Induction of forebrain glutamate neurons was described[41]. In brief, hESCs were cultured on Matrigel-coated 6-well plates for five days, growing to a density of 80% confluency. On day 0, ESC colonies were gently detached using a 1 mL pipette to form cell aggregates. Cell aggregates were suspended in T75 flasks (Greiner Bio-One, CAT#:

658195) for 7 days with 8 mL neural induction medium (NIM) consisting of DMEM/F12 (Gibco, CAT#: 21331020), 1 × N2 supplement (Gibco, CAT#: 17502048), 1 × NEAA, 2-μM SB431542 (STEMCELL, CAT#: 72232), and 2-μM DMH-1 (STEMCELL, CAT#: 100-1043). Cell aggregates were adhered to 6-well plates in the presence of NIM with 5% FBS for 6 h, and then replaced with fresh NIM. The aggregates were cultured in NIM till neural rosette formation at day 14. The rosettes were gently blown off using 1 mL pipettes and suspended in flasks with NIM for 6 days. Then, NIM was changed every five days from day 20. The neural progenitors were maintained in NIM till transplantation or immunostaining. Progenitors were digested into single cells using TrypLE for 3 min at day 33. After two additional days of incubation in NIM supplemented with 1 × B-27 (Gibco, CAT#: 17504044) and 100 nM compound E (MedChemExpress, CAT#: HY-14176), the progenitors were collected for transplantation. For immunostaining, progenitors were seeded on glass coverslips and staining was performed after one-week culture.

Stroke Model

All animal studies were performed in accordance with the institutional animal care and use committee at Duke-NUS Medical School. Ischemic strokes in adult (10-12 weeks) male SCID mice were induced through photo-thrombosis. Briefly, Rose Bengal was administered intravenously at a dose of 0.1 mg/g per mouse. Mouse skull was exposed under 3% isoflurane anesthesia. The right motor cortex (anterior-posterior [AP] = +2 mm, lateral [L] = +1 mm) received a 2.5-mm diameter illumination of cold light through the intact skull for 15 min.

Cell Transplantation

Medium for NPC transplantation contains fibrinogen and maraviroc, as described previously[17]. Stock solution of 30 mg/mL fibrinogen, 50 mg/mL maraviroc and 250

mM CaCl2 (100×) were prepared in the following manner: fibrinogen (F3879, Sigma) was dissolved in a-CSF for 1 hour at room temperature. Maraviroc was dissolved in Dimethyl Sulfoxide (DMSO) (D8418-500ML, Sigma). $CaCl_2$ (499609, Sigma) was dissolved in deionized (DI) water. All solutions were sterile filtered and stored at -20 °C for use. Fibrinogen stock solution was diluted to 10 mg/mL fibrinogen in aCSF before preparing the cocktail. Cocktail was made of 30 mg/mL maraviroc and 10 mg/mL fibrinogen in a volume ratio of 1: 9 with 2.5 mM $CaCl_2$. Animals were randomly grouped and transplanted with forebrain glutamatergic progenitors. Fifty thousand cells were resuspended in 1 μL medium and injected into the injured site ([AP] = +2 mm, [L] = +1 mm, vertical [V] = -1.5 mm, from dura).

Tissue Preparation and Immunohistochemistry

Animals were sacrificed with a lethal dose of pentobarbital (250 mg/kg) and immediately perfused with PBS followed by 4% cold paraformaldehyde (PFA). The brain samples were fixed in cold PFA overnight and immersed sequentially in 20% and 30% sucrose at 4 °C until sunk. For immunostaining, sections were incubated with blocking solution containing 10% normal donkey serum and 0.2% TritonX-100 for 1h at room temperature. Then sections were incubated with primary antibodies overnight at 4 °C.

Sections were subsequently rinsed with PBS and incubated with corresponding secondary antibodies for 1h at room temperature. Immunolabeled sections were mounted by Fluoromount-G with Hoechst.

Antibodies	Host species	Source	Identifier	Website
anti-Ctip2 1:300	Rat	Abcam	ab18465	https://www.abcam.com/ctip2-antibody-25b6-ab18465.html
anti-Fezf2 1:200	Rabbit	Abcam	ab69436	https://www.abcam.com/en-us/products/primary-antibodies/znf312-fezf2-antibody-ab69436
anti-Tbr1 1:1000	Mouse	Santa Cruz	sc-376258	https://www.scbt.com/p/tbr-1-antibody-g-5?gad_source=1&gclid=CjwKCAiAjp-7BhBZEiwAmh9rBaQ2WC6U9iknCys_ciJpDcMThNybsGv-j3_vwitgVQKNQpLGYfQ3fRoCytoQAvD_BwE
anti-Tbr1 1:1000	Rabbit	Proteintech	20932-I-AP	https://www.ptgcn.com/products/TBR1-Antibody-20932-1-AP.htm
anti-HNA 1:1000	Mouse	Merck Millipore	MAB1281	https://www.merckmillipore.com/SG/en/product/Anti-Nuclei-Antibody-clone-235-1,MM_NF-MAB1281?ReferrerURL=https%3A%2F%2Fwww.google.com%2F
anti-hNCAM 1:300	Mouse	Santa Cruz	sc-106	https://www.scbt.com/p/ncam-antibody-eric-1?gad_source=1&gclid=CjwKCAiAjp-7BhBZEiwAmh9rBZRj6B2uDx2UzbW_dSpuNIderipnTv3i5w3dPUXDaa_Py1VfnWg4ihoCFroQAvD_BwE
anti-STEM121 1:500	Mouse	Takara	Y40410	https://www.takarabio.com/products/antibodies-and-elisa/primary-antibodies-and-elisas-by-research-

				area/stem-cell-research-antibodies/stem-antibodies?catalog=Y40410
anti-Sox9 1:600	Goat	R&D Systems	AF3075	https://www.rndsystems.com/products/human-sox9-antibody_af3075
anti-NeuN 1:500	Mouse	Merck Millipore	MAB377	https://www.merckmillipore.com/CN/zh/product/Anti-NeuN-Antibody-clone-A60,MM_NF-MAB377
anti-mCherry 1:500	Rabbit	Abcam	ab167453	https://www.abcam.com/en-us/products/primary-antibodies/mcherry-antibody-ab167453
anti-WGA 1:300	Goat	Vector Labs	AS-2024-1	https://vectorlabs.com/products/anti-wheat-germ-agglutinin-wga?srsltid=AfmBOooCTOf5Z674QiZk4VFQ6gb_dO_qlSbwg-fqJWRyNpEjqryATm2x
anti-GAD67 1:500	Mouse	Merck Millipore	MAB5406-25UG	https://www.merckmillipore.com/SG/en/product/Anti-GAD67-Antibody-clone-1G10.2,MM_NF-MAB5406-25UG?ReferrerURL=https%3A%2F%2Fwww.google.com%2F
anti-vGluT1 1:500	Mouse	Invitrogen	9129S	https://www.thermofisher.com/order/genome-database/details/antibody/OSV00007G?SID=srch-srp-OSV00007G
anti-TH 1:500	Mouse	Immunostar	22941	https://www.immunostar.com/product/tyrosine-hydroxylase-antibody/
anti-ChAT 1:500	Goat	Merck Millipore	AB144P	https://www.merckmillipore.com/SG/en/product/Anti-Choline-Acetyltransferase-Antibody,MM_NF-

				AB144P?ReferrerURL=https%3A%2F%2Fwww.google.com%2F
anti-FOS 1:200	Guinea Pig	Synaptic Systems	226 308	https://www.sysy.com/product/226308
anti-Iba1 1:500	Rabbit	Wako Pure Chemical Corporation	019-19741	https://labchem-wako.fujifilm.com/us/product/detail/W01W0101-1974.html
anti-Laminin 1:1000	Mouse	Novusbio	NB300-144	https://www.novusbio.com/products/laminin-antibody_nb300-144
anti-MBP 1:500	Rabbit	Abcam	ab218011	https://www.abcam.com/en-us/products/primary-antibodies/myelin-basic-protein-antibody-epr21188-ab218011

Whole-mount Staining, Imaging and 3D Reconstruction

The protocol of whole-mount staining has been described (Renier, 2014). Briefly, transplanted mice were perfused with 20mL PBS and 20mL 4% PFA/PBS. The dissected brains and spinal cords were fixed in 4%PFA/PBS at 4°C overnight and 1hour RT with shaking, followed by wash in PBS with shaking for 30min for 3 times. Samples were dehydrated with 20%, 40%, 60%, 80%, and 100% methanol/H_2O for 1 hour each, re-washed with 100% methanol for 1 hour and chilled at 4°C. The samples were then incubated in 66% (dichloromethane) DCM / 33% methanol at RT overnight, washed twice in 100% methanol at RT and chilled at 4°C. The samples were then bleached in chilled fresh 5% H_2O_2 (1 volume 30% H_2O_2 to 5 volumes MeOH) at 4°C overnight and rehydrated with 80%, 60%, 40%, 20% methanol/H_2O and PBS for 1 hour each at RT. The samples were washed in PBS/0.2% Triton X-100 for 1 hour twice at RT and incubated in Permeabilization Solution (PBS/0.2% Triton X-100/20% DMSO/0.3 M

glycine) and then Blocking Solution (PBS/0.2% Triton X-100/10% DMSO/6% Donkey Serum) at 37°C for 2 days each. PTwH was prepared as PBS/0.2% Tween-20 with 10 μg/ml heparin. Then the samples were incubated with primary antibody in PTwH/5% DMSO/3% Donkey Serum at 37°C for 7 days and washed in PTwH for 4-5 times until the second day. Then the samples were incubated with secondary antibody in PTwH/3% Donkey Serum at 37°C for 7 days and washed in PTwH for 4-5 times until the second day. After immunolabeling, the samples were dehydrated with steps described above and incubated in 66% DCM / 33% Methanol at RT with shaking for 3 hours. Then the samples were incubated in 100% DCM for 15 min with shaking twice and incubated in DBE until imaging.

Single plane illuminated (light-sheet) image stacks were acquired using the Ultramicroscope Blaze with the following filter sets: ex 470 nm, em 525/50 nm; ex 561 nm, em 595/40 nm; ex 640 nm, em 680/30 nm; ex 785 nm, em 845/55 nm (Miltenyi Biotec). The (sample) was imaged using a 4.0x/12.0x objective lens with a magnification of (insert magnification here, the available magnification is 0.66, 1, 1.67, 2.5).

Raw image data in the form of OME-TIFFs were converted into imaris format using the Imaris File Converter version (insert version), then stitched together using the Imaris Stitcher version (insert version), and analysed using the Imaris analysis software version (insert version)

The whole-mount imaging was taken using 3D light-sheet microscopy and raw data were converted into iMaris format from Miltenyi. The imaris images were 3D reconstructed with imaris stitcher 10.2.0 (RRID:SCR_007370) for final viewing.

Retrograde Labeling

To retrogradely label the grafted neurons associated with motor control in the SC (those projecting through SC level C7), an AAV injection was performed at 5-week before collecting grafts. Specifically, mice were anesthetized and a laminectomy of the C7-T1

vertebral processes was performed. AAV-Retro (AAV-CAG-hChR2-H134R-tdTomato) was injected at one site per segment within the ipsilateral (right side) C7-T1 spinal segments (300 nL/injection) at 0.9 μm below the dorsal spinal cord surface at each site (rate = 100 nL/min). In the same surgical session, AAV-Retro (pAAV-hSyn-HI-GFP-WPRE-SV40) was injected into the corresponding contralateral site, and 300 nl virus was injected at same depth. A total of three animals were sacrificed for snRNA sequencing.

For multiple-site retrograde tracing, 20 bp barcode sequence for identity was inserted before SV40 polyA in pAAV-hSyn-HI-GFP-WPRE-SV40 (OBiO Technology).

Barcode-S for striatal identity: GCTACGCCATCGCAAGGCCT

Barcode-C for cortex (S1Tr) identity: CCAAGCGTATGCTACGCGTT

Barcode-T for thalamus identity: AGCCTTGCATCGCATCAAGG

Barcode-M for MY identity: TACTGAGTCGCAAGCGCTCC

Mice were anesthetized with 3% isoflurane. In the same surgical session, the barcode-AAV was injected (500 nL/injection, rate = 100 nL/min) at the following coordinates from Bregma: striatum (AP = 0.26 mm, ML = 2.00 mm, DV = -2.80 mm), cortex (AP = -1.46 mm, ML = 1.50 mm, DV = -1.20 mm), thalamus (AP = -0.95 mm, ML = 1.10 mm, DV = -3.50 mm), SC (AP = -8.30 mm, ML = 0.00 mm, DV = -5.20 mm). The micropipette was left in tissue for 10 min before slowly withdrawn. A total of three mice were perfused by cold PBS, and the grafts were dissociated to single nuclei for snRNA-seq. The brain and SC were collected for immunostaining.

snRNA Sequencing Library Preparation and Sequencing

The single nuclei RNA-seq libraries were constructed using GEXSCOPE™ Single Nuclei RNAseq Library Kit (Singleron Biotechnologies) according to the manufacturer´s instructions. Briefly, for each library, the nuclei suspension of specified

concentration was loaded onto a microfluidic chip for capture. The single-nuclei capture, lysis and mRNA capture steps were automated using Singleron Matrix NEOTM system. The final single-cell RNA sequencing libraries were sequenced on Illumina NovaSeqX plus 25B flowcell with paired-end 150 bp.

Transcriptome Data Pre-processing

Fastq files were preprocessed using the CeleScope® tools (version 2.0.7); www.github.com/singleron-RD/CeleScope, Singleron Biotechnologies), to generate raw data using default parameters. Briefly, cellular barcodes in Read 1 were used to demultiplex and identify reads of the same cell origin. Low quality and adapter sequences were removed using cutadapt (version 3.7). The mapping was done using STARSOLO (https://github.com/alexdobin/STAR/blob/master/docs/STARsolo.md) against human genome build (GRCh38) with ENSEMBL Gene Annotation (Version 99) with gene sequences of GFPCRE1, GFPCRE2, GFPCRE3, GFPCRE4, and CHR2RFP included. The reads were assigned to genes using the featureCount tool (https://subread.sourceforge.net) and the cell calling was performed by fitting a negative bimodal distribution and determining the threshold between empty wells and cell-associated wells. The gene count matrix was then generated, providing the number of unique molecular identifier (UMI) for each gene and cell. https://cutadapt.readthedocs.io/en/stable/installation.html).

Single-nuclei Data Analysis

Downstream analysis was done using the snRNA analysis pipeline CeleScoot 1.2.2 (https://github.com/singleron-RD/scrna). QC metrics, such as the number of genes detected per cell (nFeature_RNA) and the percentage of mitochondrial UMI (percent_mt) were extracted from the gene count matrix with the function calculate_qc_metrics. Nuclei with high percentage of mitochondrial counts

(>20%) were filtered out. The cells with a high number of detected genes (>5000) were excluded to remove possible doublets. Cell debris characterized by low detected genes (<200) was also excluded from the data analysis.

All subsequent analysis was performed using R (version 4.4.0) package Seurat (version 5.0.3). The raw count matrices were normalized by natural-log transformation with a scale factor of 10000. Dimensionality reduction using principal component analysis (PCA) was performed, and clusters of nuclei were identified in PCA space by shared nearest-neighbour graph construction and modularity detection implemented by the FindNeighbors and FindClusters functions using a dataset dimension of 30 and resolution of 1.0. The dataset was embedded for visualization with UMAP. Marker genes for each cluster were calculated using FindMarkers with default parameters based on normalized data, and filtered with the criteria: p-value < 0.05, |log2FC| > 1 and percentage of ident.1 > 10%. We identified cell types by the expression of known marker genes. Glutamatergic neurons were identified by the expression of SYT1 and SATB2. Deep layer neurons were identified by co-expression of Ctip2 (BCL11B) and Fezf2 or TBR1. Upper layer neurons were identified by the expression of Brn2 (POU3F2). GABAergic neurons were identified by the expression of GAD1. Astrocytes were identified by the expression of AQP4 and SLC1A3. Oligodendrocytes were identified by the expression of OLIG1 and OLIG2. Proliferating cells were identified by KI67 (MKI67). To better understand the cell population, we integrated the dataset to the human adult M1 cortex dataset using the Anchor-based CCA integration in Seurat. Only genes detected in both datasets were included in comparison. Our cells were defined using the label from the reference clusters where they were overlapped. Heatmaps were drawn with 50 cells randomly selected from each cluster. Gene Ontology (GO) enrichment analysis was performed using enrichR.

Trajectory analysis

We performed UMAP dimension reduction at the trajectory level with the integration function from Seurat, using all genes. Each cell was assigned a pseudotime value based on its position along the trajectory using monocle3/v1.3.7 function

"order_cells()"[42].For the integrated endogenous dataset, each cell was assigned a pseudotime value along the trajectory within the whole dataset. For the integrated endogenous-graft dataset, cells were subset to each subtype and each cell was assigned a pseudotime value based on its position along the trajectory within the certain subtype.

Identification of transcriptional codes by machine learning

Single-cell RNA sequencing data was processed and analyzed using Python. Gene expression data was extracted from the AnnData object, with raw counts converted into a dense array format. Cells were classified based on their source, distinguishing grafted cells from endogenous cells. Canonical correlation analysis (CCA) embeddings, stored in `obsm['X_cca']`, were concatenated with gene expression features to create a combined feature matrix.

Feature selection was performed in two steps. First, the top 100 features (genes) were calculated using the `SelectKBest` method with the `f_classif` statistical test. Subsequently, L1-regularized logistic regression (Lasso) was applied to further refine the feature set, retaining only genes with nonzero coefficients.

The refined feature set was used to train a logistic regression model with L1 regularization (C=0.01) on 80% of the data, while the remaining 20% was used for testing. The model was trained using the `liblinear` solver. The results were cross-validated by Bayesian Additive regression trees. Performance was assessed using receiver operating characteristic (ROC) curve analysis, and the area under the curve (AUC) was computed to evaluate classification accuracy.

Neuron Prediction and Output

The trained logistic regression model was applied to the full dataset to predict cell source probabilities. Cells with a probability greater than 0.5 were classified as grafted. The above pipeline was applied iteratively to multiple cell subtypes, with subtypes

identified based on the `brief_id` field. The analysis was conducted separately for each subtype, ensuring subtype-specific feature selection, model training, and visualization.

CTIP2-kd ESC Line

Human Ctip2 (BCL11B) 29mer shRNA plasmids (pRS-hU6-Ctip2shRNA-GFP-SV40-Puro) and non-effective 29-mer scrambled shRNA cassette in pRS Vector were obtained from OriGene (CAT#: TR306424). The lentivirus was generated in the HEK 293FT cell line by transfecting with the packaging and backbone plasmids. HEK 293FT cells were cultured in DMEM high glucose (Cytiva CAT#: SH30081.01) with 10% FBS. The supernatant was collected after 3-day culture. Viral particles were concentrated by ultracentrifugation at 25 000 rpm for 2.5 h at 4 °C. The viral particles were resuspended in DMEM. The H9 ESCs were infected with the lentivirus (MOI = 50) overnight at 37 °C. The infected ESCs were sparsely cultured in the 60-mm dish (D8054, Sigma) for 3 days. The GFP labeled clones were selected for culture. The cell line was identified by staining for Ctip2 as above described.

Anterograde tracing

mWGA-mCherry. Codon-optimized WGA (mWGA) was synthesized at IDT and fused with RFPs. We used mCherry to tag the C-terminus of mWGA. These vectors are available at Addgene for requests. The reference sequence for mWmC cDNA was optimized as below[18]:

ATGGAGACCGACACCCTGCTGCTGTGGGTGCTTCTGCTGTGGGTCCCTGGC
AGCACTGGCGATGGGCCTGTGATGACCGCCCAAGCTCAGAGGTGCGGCGA
GCAAGGCAGCAACATGGAGTGCCCTAATAACTTGTGCTGCTCTCAGTACG
GCTATTGCGGCATGGGTGGCGACTACTGCGGCAAGGGCTGTCAGAACGGC
GCCTGCTGGACTAGCAAGAGGTGCGGCTCCCAAGCCGGCGGTGCCACCTG
CCCTAACAATCACTGTTGCTCACAGTACGGTCACTGCGGCTTCGGCGCCG

AGTACTGTGGGGCTGGTTGCCAAGGCGGCCCTTGTAGGGCCGATATCAAG
TGCGGCAGTCAAAGCGGCGGCAAATTGTGCCCTAACAACCTGTGCTGCTC
TCAGTGGGGTTTCTGCGGACTGGGAAGCGAGTTTTGCGGCGGCGGGTGTC
AATCCGGCGCTTGTAGCACCGACAAGCCTTGCGGCAAGGACGCCGGCGGA
AGGGTGTGCACCAACAACTACTGCTGCAGCAAATGGGGATCGTGTGGCAT
AGGCCCTGGCTACTGCGGCGCTGGGTGTCAGTCGGGCGGCTGCGACGCCG
CTAGGGACCCTCCTGTGGCAAGCGCCACCATGGTGAGCAAGGGCGAGGA
GGACAACATGGCCATCATCAAGGAGTTCATGAGGTTCAAGGTGCACATGG
AGGGCAGCGTGAACGGCCACGAGTTCGAGATCGAGGGCGAGGGCGAGGG
AAGGCCTTACGAGGGCACACAGACCGCCAAGCTGAAGGTGACCAAGGGC
GGCCCTCTGCCTTTCGCCTGGGACATCCTGAGCCCTCAGTTCATGTACGGC
AGCAAGGCCTACGTGAAGCACCCTGCCGACATCCCTGACTACCTGAAGCT
GAGCTTCCCTGAGGGCTTCAAGTGGGAGAGGGTGATGAACTTCGAGGACG
GCGGCGTGGTGACCGTGACCCAAGACAGCAGCCTGCAAGACGGCGAGTT
CATCTACAAGGTGAAGCTGAGGGGCACCAACTTCCCTAGCGACGGCCCTG
TGATGCAGAAGAAGACCATGGGCTGGGAGGCAAGCAGCGAGAGGATGTA
CCCTGAGGACGGCGCCCTGAAGGGCGAGATCAAGCAGAGGCTGAAGCTG
AAGGACGGCGGCCACTACGACGCCGAGGTGAAGACCACCTACAAGGCCA
AGAAGCCTGTGCAGCTGCCTGGCGCCTACAACGTGAACATCAAGCTGGAC
ATCACAAGCCACAACGAGGACTACACCATCGTGGAGCAGTACGAGAGGG
CCGAGGGAAGGCACAGCACCGGCGGCATGGACGAGCTGTACAAGTGA

For adult motor cortex tracing, animals were anesthetized with isoflurane and stereotaxically injected (primary motor cortex: AP = 0.85mm, ML = 1.50 mm, DV = -2.00 mm) with AAV-CAG-mWmC (OBiO Technology). The viruses, animal lines and injection sites used are as follows. For Figure S4C, AAV-CAG-mWmC (500 nl) (100 nl/ min) was injected into the NSG mice. A total of five mice were sacrificed for immunostaining at four weeks after AAV injection.

To generate the SYN1-mWmC hESC line, the AAVS1-puro-hSyn-mWmC construct was integrated into the AAVS1 locus of H9 hESCs using the CRISPR/Cas9 system

(TrueCut™ Cas9 Protein v2, A36497, Life Technologies) via transfection with the NEON 10 µL Transfection Kit (MPK1025, Life Technologies).

The single guide RNA (sgRNA) sequence used for targeting the AAVS1 locus was as follows: 5`-mU*mG*mU*rCrCrCrUrArGrUrGrGrCrCrCrCrArCrUrGrGrUrUrUrUrArGrArGrCrUrAr GrArArArUrArGrCrArArGrUrUrArArArArUrArArGrGrCrUrArGrUrCrCrGrUrUrArUrCrArArCrUrUrGrArArArArArGrUrGrGrCrArCrCrGrArGrUrCrGrGrUrGrCmU*mU*mU*rU-3`

The DREADD hESC line was described previously[43]. To generate the DREADD-CAG-mWmC and DREADD-CAG-mWmC-GFP hESC lines, the DREADD hESC line was infected with the lentivirus. Specifically, the mWmC cDNA was inserted into plasmid lenti-CAG-WPRE or lenti-CAG-IRES-GFP-WPRE. The lenti-CAG-mWmC-GFP and lenti-CAG-mWmC virus were generated as described in "Ctip2-kd ESC Line". The DREADD hESCs were infected with the lentivirus (MOI = 100) overnight at 37 °C. The infected ESCs were sparsely cultured in the 60-mm dish. After three-day culture, six clones for each line were collected separately into a 24-well plate. The hESCs were cultured on coverslips for WGA staining to identify the cell line.

Imaging and Cellular Quantification

Serial coronal (1.54 mm to -0.22 mm from Bregma) sections were collected on a freezing microtome at a 30-µm thickness and stored at -20 °C. To quantify the cell number of Ctip2, Fezf2, Tbr1, HNA, Sox9, WGA, mCherry, GFP, FOS, Hoechst, vGluT1, GAD67, TH, ChAT, and NeuN positive cells, one brain slice was selected from every 6 serial slices for stereological counting on a Zeiss M1 Microscope with Stereo Investigator software (MBF Bioscience). In brief, immunolabeled slices were scanned on Zeiss M1 Microscope, grafts area was outlined manually, and then

corresponding fluorescence labeled cells were unbiasedly counted. Data were replicated 4 to 5 times per group. All data were expressed as means±SEM.

To quantify the population of Ctip2, Fezf2, and Tbr1 expressing cells among total HNA^+ cells on 16mm coverslips (Marienfeld Superior), all coverslips were scanned and captured by 20× objective with a confocal microscope (Nikon), and then was counted with the ImageJ software. Data were replicated three times. All data were expressed as means±SEM.

Behavioral Tests

Before inducing stroke models, mice were screened using NeurodegenScan Suite (Clever Sys Inc.) for gait analysis. The mice were placed on a stationary treadmill, which accelerated to 8 m/s within 5 seconds. Mice with speeds ranging from 10–12 m/s were selected for inducing stroke model.

Behavioral tests were conducted 12 months after transplantation. During these tests, mice were placed on a stationary treadmill that accelerated to 8 m/s within 5 seconds. One week prior to the formal test, the mice underwent training sessions every two days. Each training session consisted of three practices, with 30 minutes between each practice. For each animal, a 20-second video was recorded for data analysis, with 20–25 animals per group. Each animal was tested three times for subsequent analysis using nonlinear dimensionality reduction. GaitScan Analysing System (TreadScan v.4) outputs the detailed results of these parameters from analysis into Microsoft Excel files and gives statistical results.

For DCZ administration, mice transplanted with hM4Di-neurons underwent behavioral testing. One hour after the initial test, the mice received an intraperitoneal injection of DCZ. Behavioral testing was repeated 40 minutes after the DCZ administration.

QUANTIFICATION AND STATISTICAL ANALYSIS

A two-tailed Student's t-test was used for the pairwise comparison between two groups. The rest of the data were analyzed using a one-way or two-way ANOVA as appropriate. Error bars in all figures represent means ± SEM. Differences were considered statistically significant at a P value of less than 0.05. All data were analyzed using GraphPad Prism.

ACKNOWLEDGMENTS

These studies were supported in part by a Duke/Duke-NUS Pilot grant, National Medical Research Council of Singapore (MOH-000207, MOH-000212), Open Fund-Young Individual Research Grant (OFYIRG23jan-0031), and Khoo Postdoctoral Fellowship Award (Duke-NUS-KPFA/2021/0047). We thank Qiang Yuan, Ye Sing Tan, Xianfeng Tian, Chung Hock Lee, and Mynn Michele Dy Varela for dedicated technical assistance.

AUTHOR CONTRIBUTIONS

Conception and design of work, SC.Z., and ZF.W.; stroke model, ZF.W. and DY.Z.; cell transplantation, ZF.W.; cell culture, ZF.W. and DY.Z.; animal breeding, ZF.W. and DY.Z.; lentivirus production, ZF.W.; cell line generation: ZF.W. and P.J.K.; data collection, ZF.W. and DY.Z.; data analysis and interpretation, ZF.W., DY.Z., and SC.Z.; drafting the article, ZF.W. and SC.Z..

DECLARATION OF INTERESTS

The authors declare no competing interests.

Reference

1. Espuny-Camacho, I., Michelsen, K.A., Gall, D., Linaro, D., Hasche, A., Bonnefont, J., Bali, C., Orduz, D., Bilheu, A., Herpoel, A., et al. (2013).

Pyramidal neurons derived from human pluripotent stem cells integrate efficiently into mouse brain circuits in vivo. Neuron *77*, 440-456. 10.1016/j.neuron.2012.12.011.

2. Kitahara, T., Sakaguchi, H., Morizane, A., Kikuchi, T., Miyamoto, S., and Takahashi, J. (2020). Axonal Extensions along Corticospinal Tracts from Transplanted Human Cerebral Organoids. Stem Cell Reports *15*, 467-481. 10.1016/j.stemcr.2020.06.016.
3. Cao, S.Y., Yang, D., Huang, Z.Q., Lin, Y.H., Wu, H.Y., Chang, L., Luo, C.X., Xu, Y., Liu, Y., and Zhu, D.Y. (2023). Cerebral organoids transplantation repairs infarcted cortex and restores impaired function after stroke. NPJ Regen Med *8*, 27. 10.1038/s41536-023-00301-7.
4. Kebschull, J.M., Garcia da Silva, P., Reid, A.P., Peikon, I.D., Albeanu, D.F., and Zador, A.M. (2016). High-Throughput Mapping of Single-Neuron Projections by Sequencing of Barcoded RNA. Neuron *91*, 975-987. 10.1016/j.neuron.2016.07.036.
5. Xu, P., Peng, J., Yuan, T., Chen, Z., He, H., Wu, Z., Li, T., Li, X., Wang, L., Gao, L., et al. (2024). High-throughput mapping of single-neuron projection and molecular features by retrograde barcoded labeling. Elife *13*. 10.7554/eLife.85419.
6. Klingler, E., Tomasello, U., Prados, J., Kebschull, J.M., Contestabile, A., Galiñanes, G.L., Fièvre, S., Santinha, A., Platt, R., Huber, D., et al. (2021). Temporal controls over inter-areal cortical projection neuron fate diversity. Nature *599*, 453-457. 10.1038/s41586-021-04048-3.
7. Van Battum, E.Y., Brignani, S., and Pasterkamp, R.J. (2015). Axon guidance proteins in neurological disorders. Lancet Neurol *14*, 532-546. 10.1016/s1474-4422(14)70257-1.
8. Linaro, D., Vermaercke, B., Iwata, R., Ramaswamy, A., Libé-Philippot, B., Boubakar, L., Davis, B.A., Wierda, K., Davie, K., Poovathingal, S., et al. (2019). Xenotransplanted Human Cortical Neurons Reveal Species-Specific Development and Functional Integration into Mouse Visual Circuits. Neuron *104*, 972-986.e976. 10.1016/j.neuron.2019.10.002.
9. Michelsen, K.A., Acosta-Verdugo, S., Benoit-Marand, M., Espuny-Camacho, I., Gaspard, N., Saha, B., Gaillard, A., and Vanderhaeghen, P. (2015). Area-specific reestablishment of damaged circuits in the adult cerebral cortex by cortical neurons derived from mouse embryonic stem cells. Neuron *85*, 982-997. 10.1016/j.neuron.2015.02.001.
10. Falkner, S., Grade, S., Dimou, L., Conzelmann, K.K., Bonhoeffer, T., Götz, M., and Hübener, M. (2016). Transplanted embryonic neurons integrate into adult neocortical circuits. Nature *539*, 248-253. 10.1038/nature20113.
11. Xiong, M., Tao, Y., Gao, Q., Feng, B., Yan, W., Zhou, Y., Kotsonis, T.A., Yuan, T., You, Z., Wu, Z., et al. (2021). Human Stem Cell-Derived Neurons Repair Circuits and Restore Neural Function. Cell Stem Cell *28*, 112-126.e116. 10.1016/j.stem.2020.08.014.

12. Fiorenzano, A., Storm, P., Sozzi, E., Bruzelius, A., Corsi, S., Kajtez, J., Mudannayake, J., Nelander, J., Mattsson, B., Åkerblom, M., et al. (2024). TARGET-seq: Linking single-cell transcriptomics of human dopaminergic neurons with their target specificity. Proc Natl Acad Sci U S A *121*, e2410331121. 10.1073/pnas.2410331121.
13. Revah, O., Gore, F., Kelley, K.W., Andersen, J., Sakai, N., Chen, X., Li, M.Y., Birey, F., Yang, X., Saw, N.L., et al. (2022). Maturation and circuit integration of transplanted human cortical organoids. Nature *610*, 319-326. 10.1038/s41586-022-05277-w.
14. Tornero, D., Tsupykov, O., Granmo, M., Rodriguez, C., Grønning-Hansen, M., Thelin, J., Smozhanik, E., Laterza, C., Wattananit, S., Ge, R., et al. (2017). Synaptic inputs from stroke-injured brain to grafted human stem cell-derived neurons activated by sensory stimuli. Brain *140*, 692-706. 10.1093/brain/aww347.
15. Palma-Tortosa, S., Tornero, D., Grønning Hansen, M., Monni, E., Hajy, M., Kartsivadze, S., Aktay, S., Tsupykov, O., Parmar, M., Deisseroth, K., et al. (2020). Activity in grafted human iPS cell-derived cortical neurons integrated in stroke-injured rat brain regulates motor behavior. Proc Natl Acad Sci U S A *117*, 9094-9100. 10.1073/pnas.2000690117.
16. Rust, R., Nih, L.R., Liberale, L., Yin, H., El Amki, M., Ong, L.K., and Zlokovic, B.V. (2024). Brain repair mechanisms after cell therapy for stroke. Brain *147*, 3286-3305. 10.1093/brain/awae204.
17. Wang, Z., Zheng, D., Tan, Y.S., Yuan, Q., Yuan, F., and Zhang, S.C. (2023). Enabling Survival of Transplanted Neural Precursor Cells in the Ischemic Brain. Adv Sci (Weinh) *10*, e2302527. 10.1002/advs.202302527.
18. Tsai, N.Y., Wang, F., Toma, K., Yin, C., Takatoh, J., Pai, E.L., Wu, K., Matcham, A.C., Yin, L., Dang, E.J., et al. (2022). Trans-Seq maps a selective mammalian retinotectal synapse instructed by Nephronectin. Nat Neurosci *25*, 659-674. 10.1038/s41593-022-01068-8.
19. Lemon, R.N. (2008). Descending pathways in motor control. Annu Rev Neurosci *31*, 195-218. 10.1146/annurev.neuro.31.060407.125547.
20. Zhang, Z., Su, J., Tang, J., Chung, L., Page, J.C., Winter, C.C., Liu, Y., Kegeles, E., Conti, S., Zhang, Y., et al. (2024). Spinal projecting neurons in rostral ventromedial medulla co-regulate motor and sympathetic tone. Cell *187*, 3427-3444.e3421. 10.1016/j.cell.2024.04.022.
21. Sinopoulou, E., Rosenzweig, E.S., Conner, J.M., Gibbs, D., Weinholtz, C.A., Weber, J.L., Brock, J.H., Nout-Lomas, Y.S., Royz, E., Takashima, Y., et al. (2022). Rhesus macaque versus rat divergence in the corticospinal projectome. Neuron *110*, 2970-2983.e2974. 10.1016/j.neuron.2022.07.002.
22. Gao, L., Liu, S., Gou, L., Hu, Y., Liu, Y., Deng, L., Ma, D., Wang, H., Yang, Q., Chen, Z., et al. (2022). Single-neuron projectome of mouse prefrontal cortex. Nat Neurosci *25*, 515-529. 10.1038/s41593-022-01041-5.
23. Musall, S., Sun, X.R., Mohan, H., An, X., Gluf, S., Li, S.J., Drewes, R., Cravo, E., Lenzi, I., Yin, C., Kampa, B.M., and Churchland, A.K. (2023). Pyramidal

cell types drive functionally distinct cortical activity patterns during decision-making. Nat Neurosci *26*, 495-505. 10.1038/s41593-022-01245-9.

24. Bakken, T.E., Jorstad, N.L., Hu, Q., Lake, B.B., Tian, W., Kalmbach, B.E., Crow, M., Hodge, R.D., Krienen, F.M., Sorensen, S.A., et al. (2021). Comparative cellular analysis of motor cortex in human, marmoset and mouse. Nature *598*, 111-119. 10.1038/s41586-021-03465-8.
25. Luo, Y., Shepherd, I., Li, J., Renzi, M.J., Chang, S., and Raper, J.A. (1995). A family of molecules related to collapsin in the embryonic chick nervous system. Neuron *14*, 1131-1140. 10.1016/0896-6273(95)90261-9.
26. Brose, K., Bland, K.S., Wang, K.H., Arnott, D., Henzel, W., Goodman, C.S., Tessier-Lavigne, M., and Kidd, T. (1999). Slit proteins bind Robo receptors and have an evolutionarily conserved role in repulsive axon guidance. Cell *96*, 795-806. 10.1016/s0092-8674(00)80590-5.
27. Jaworski, A., and Tessier-Lavigne, M. (2012). Autocrine/juxtaparacrine regulation of axon fasciculation by Slit-Robo signaling. Nat Neurosci *15*, 367-369. 10.1038/nn.3037.
28. Ashrafi, S., Betley, J.N., Comer, J.D., Brenner-Morton, S., Bar, V., Shimoda, Y., Watanabe, K., Peles, E., Jessell, T.M., and Kaltschmidt, J.A. (2014). Neuronal Ig/Caspr recognition promotes the formation of axoaxonic synapses in mouse spinal cord. Neuron *81*, 120-129. 10.1016/j.neuron.2013.10.060.
29. Arlotta, P., Molyneaux, B.J., Chen, J., Inoue, J., Kominami, R., and Macklis, J.D. (2005). Neuronal subtype-specific genes that control corticospinal motor neuron development in vivo. Neuron *45*, 207-221. 10.1016/j.neuron.2004.12.036.
30. Baker, A., Kalmbach, B., Morishima, M., Kim, J., Juavinett, A., Li, N., and Dembrow, N. (2018). Specialized Subpopulations of Deep-Layer Pyramidal Neurons in the Neocortex: Bridging Cellular Properties to Functional Consequences. J Neurosci *38*, 5441-5455. 10.1523/jneurosci.0150-18.2018.
31. Nano, P.R., Fazzari, E., Azizad, D., Nguyen, C.V., Wang, S., Kan, R.L., Wick, B., Haeussler, M., and Bhaduri, A. (2023). A Meta-Atlas of the Developing Human Cortex Identifies Modules Driving Cell Subtype Specification. bioRxiv. 10.1101/2023.09.12.557406.
32. Jaworski, A., Long, H., and Tessier-Lavigne, M. (2010). Collaborative and specialized functions of Robo1 and Robo2 in spinal commissural axon guidance. J Neurosci *30*, 9445-9453. 10.1523/jneurosci.6290-09.2010.
33. Zheng, B., and Tuszynski, M.H. (2023). Regulation of axonal regeneration after mammalian spinal cord injury. Nat Rev Mol Cell Biol *24*, 396-413. 10.1038/s41580-022-00562-y.
34. Parmar, M., Grealish, S., and Henchcliffe, C. (2020). The future of stem cell therapies for Parkinson disease. Nat Rev Neurosci *21*, 103-115. 10.1038/s41583-019-0257-7.
35. Ceto, S., Sekiguchi, K.J., Takashima, Y., Nimmerjahn, A., and Tuszynski, M.H. (2020). Neural Stem Cell Grafts Form Extensive Synaptic Networks that

Integrate with Host Circuits after Spinal Cord Injury. Cell Stem Cell *27*, 430-440.e435. 10.1016/j.stem.2020.07.007.

36. Steinbeck, J.A., Choi, S.J., Mrejeru, A., Ganat, Y., Deisseroth, K., Sulzer, D., Mosharov, E.V., and Studer, L. (2015). Optogenetics enables functional analysis of human embryonic stem cell-derived grafts in a Parkinson's disease model. Nat Biotechnol *33*, 204-209. 10.1038/nbt.3124.
37. Uzquiano, A., Kedaigle, A.J., Pigoni, M., Paulsen, B., Adiconis, X., Kim, K., Faits, T., Nagaraja, S., Antón-Bolaños, N., Gerhardinger, C., et al. (2022). Proper acquisition of cell class identity in organoids allows definition of fate specification programs of the human cerebral cortex. Cell *185*, 3770-3788.e3727. 10.1016/j.cell.2022.09.010.
38. Velasco, S., Kedaigle, A.J., Simmons, S.K., Nash, A., Rocha, M., Quadrato, G., Paulsen, B., Nguyen, L., Adiconis, X., Regev, A., Levin, J.Z., and Arlotta, P. (2019). Individual brain organoids reproducibly form cell diversity of the human cerebral cortex. Nature *570*, 523-527. 10.1038/s41586-019-1289-x.
39. Jgamadze, D., Lim, J.T., Zhang, Z., Harary, P.M., Germi, J., Mensah-Brown, K., Adam, C.D., Mirzakhalili, E., Singh, S., Gu, J.B., et al. (2023). Structural and functional integration of human forebrain organoids with the injured adult rat visual system. Cell Stem Cell *30*, 137-152.e137. 10.1016/j.stem.2023.01.004.
40. Doerr, J., Schwarz, M.K., Wiedermann, D., Leinhaas, A., Jakobs, A., Schloen, F., Schwarz, I., Diedenhofen, M., Braun, N.C., Koch, P., et al. (2017). Whole-brain 3D mapping of human neural transplant innervation. Nat Commun *8*, 14162. 10.1038/ncomms14162.
41. Zhang, X., Huang, C.T., Chen, J., Pankratz, M.T., Xi, J., Li, J., Yang, Y., Lavaute, T.M., Li, X.J., Ayala, M., et al. (2010). Pax6 is a human neuroectoderm cell fate determinant. Cell Stem Cell *7*, 90-100. 10.1016/j.stem.2010.04.017.
42. Cao, J., Spielmann, M., Qiu, X., Huang, X., Ibrahim, D.M., Hill, A.J., Zhang, F., Mundlos, S., Christiansen, L., Steemers, F.J., Trapnell, C., and Shendure, J. (2019). The single-cell transcriptional landscape of mammalian organogenesis. Nature *566*, 496-502. 10.1038/s41586-019-0969-x.
43. Chen, Y., Xiong, M., Dong, Y., Haberman, A., Cao, J., Liu, H., Zhou, W., and Zhang, S.C. (2016). Chemical Control of Grafted Human PSC-Derived Neurons in a Mouse Model of Parkinson's Disease. Cell Stem Cell *18*, 817-826. 10.1016/j.stem.2016.03.014.

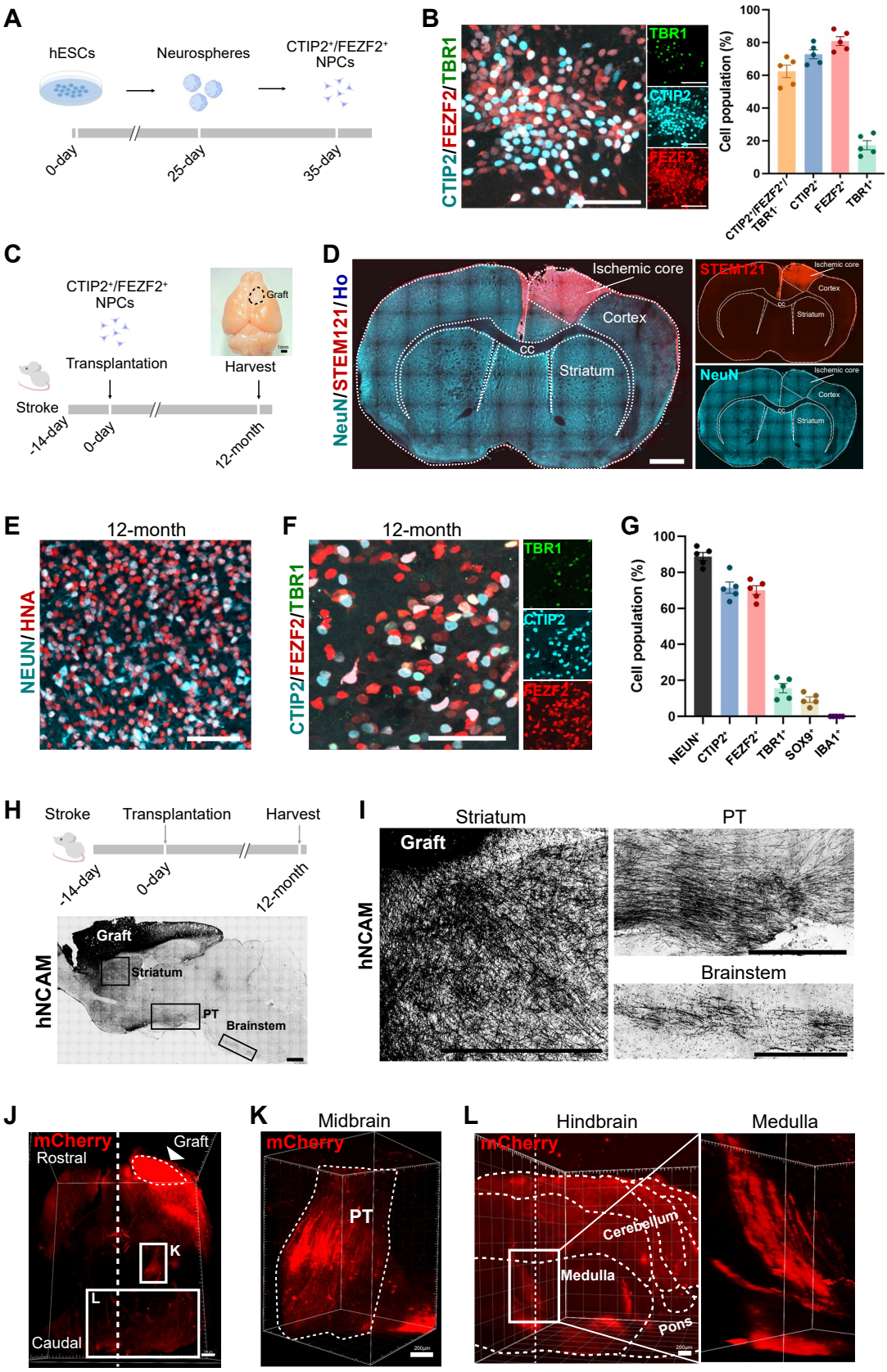

Figure 1. Transplanted human cortical neurons reconstitute the damaged cortex and project axons to subcortical regions.

(A) Cartoon outlining the differentiation of the human cortical NPCs from hESCs.
(B) Immunostaining for CTIP2, FEZF2, and TBR1 showing the cell population of induced human cortical NPCs. Quantification on the right panel; n=5 independent samples. Scale bars, 200μm.
(C) Experimental strategy for transplantation of the human cortical NPCs in stroke mice. The samples were collected at 12 months after transplantation. Scale bars, 1mm.
(D) Immunostaining with NeuN and STEM121(human cell marker) shows that the transplanted NPCs became NeuN+ neurons and filled the ischemic cavity at 12 months post-transplantation. Scale bars, 1mm.
(E) Immunostaining shows co-labelling of NEUN and human nuclear antigen (HNA) in transplanted neurons at 12 months post-transplantation. Scale bars, 200μm.
(F) Immunostaining for CTIP2, FEZF2, and TBR1 on transplanted neurons at 12 months post-transplantation. Scale bars, 100μm.
(G) Quantification for (F) shows the cell population of transplanted neurons at 12 months post-transplantation. n=5 mice.
(H) Immunostaining for hNCAM showing axonal projections of transplanted neurons in mature mouse brains.
(I) Magnification of (H) showing the axon projection by grafted neurons in the striatum, pyramidal tract (PT) and brainstem.
(J to L) 3D reconstructed images of mCherry showing axon bundle derived from grafts neurons in the transverse plane (J), midbrain (K), and hindbrain (L). Scale bars, 700μm in (J), 200μm in (K) and (L).
All Data are represented as mean±SEM.

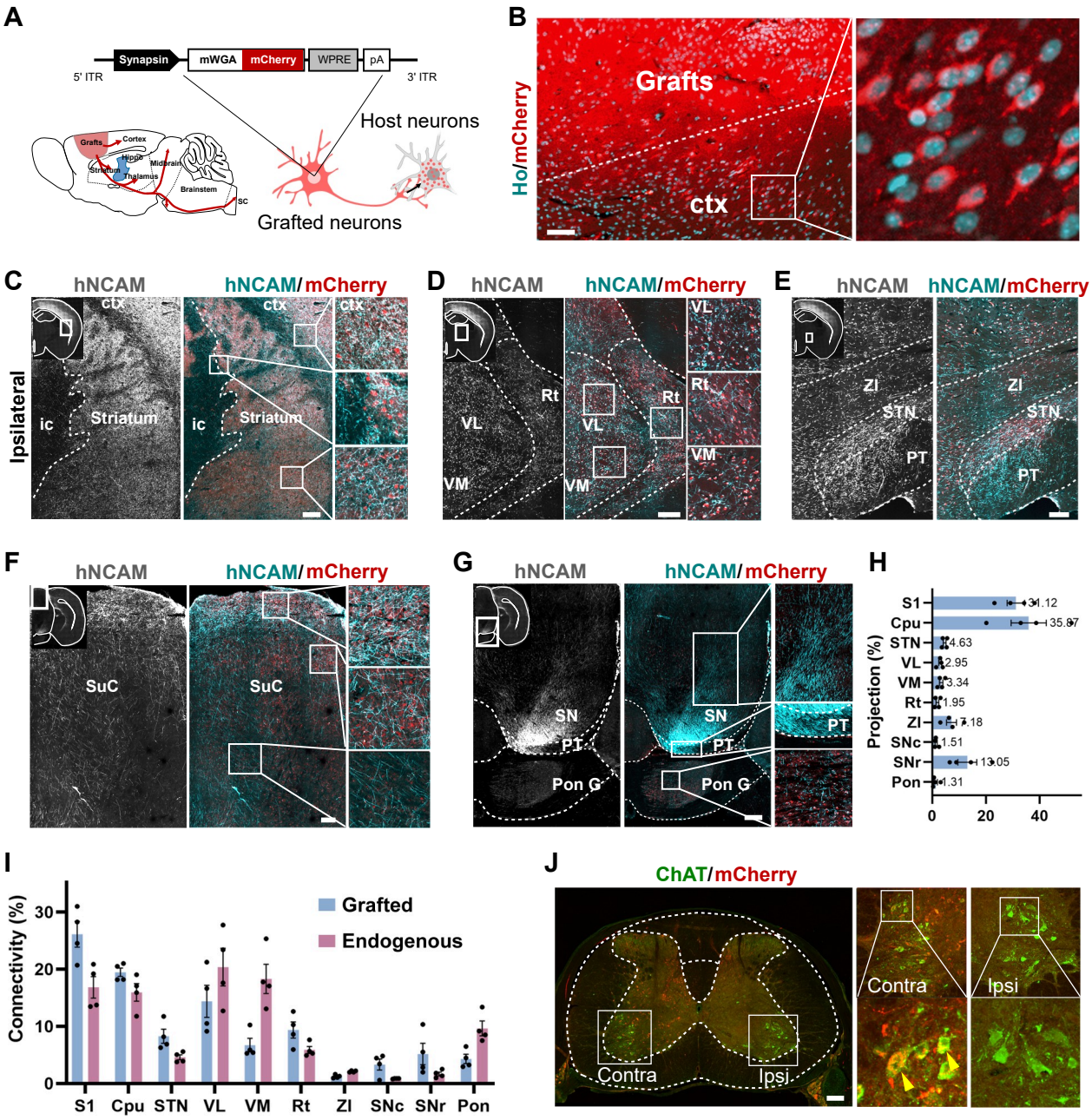

Figure 2. Post-synaptic connectivity is mapped by anterograde tracing.

(A) Cartoon illustrating the generation of the hSyn-mWmC hESC line for anterograde tracing in the transplanted brain.

(B) Immunostaining for mCherry showed the presence of mWmC in host neurons in the intact cortex adjacent to the graft. Scale bars, 100μm.

(C to G) Immunostaining for hNCAM and mCherry showing axons of grafted neurons (hNCAM+) and mCherry labeled host neurons in ipsilateral S1 and striatum (C), thalamus (D), ZI and STN (E), SuC (F), Pon G and SN (G). S1, primary somatosensory cortex. ic, internal capsule. VL, ventrolateral thalamic nucleus. Rt, reticular thalamic nucleus. ZI, zona incerta. STN, subthalamic nucleus. PT, pyramidal tract. SuC, superior colliculus. SN, substantia nigra. Pon G, pontine grey. Scale bars, 100μm.

(H) Quantification of axon projection by grafted cells in mature brains. n=4-5 mice. Data are represented as mean±SEM.

(I) Quantification of output connections of transplanted neurons (blue) and endogenous corticospinal motor neurons (purple). The connectivity ratio is shown for all brain regions receiving synaptic input from transplanted neurons at 12-month, compared to endogenous neurons in intact M1(see Figure 7B). n=4 mice per group. Data are represented as mean±SEM.

(J) Immunostaining showing WGA-labeled, ChAT-expressing host neurons in the spinal cord. Dot plot of top marker genes. Insets are magnified on the right.

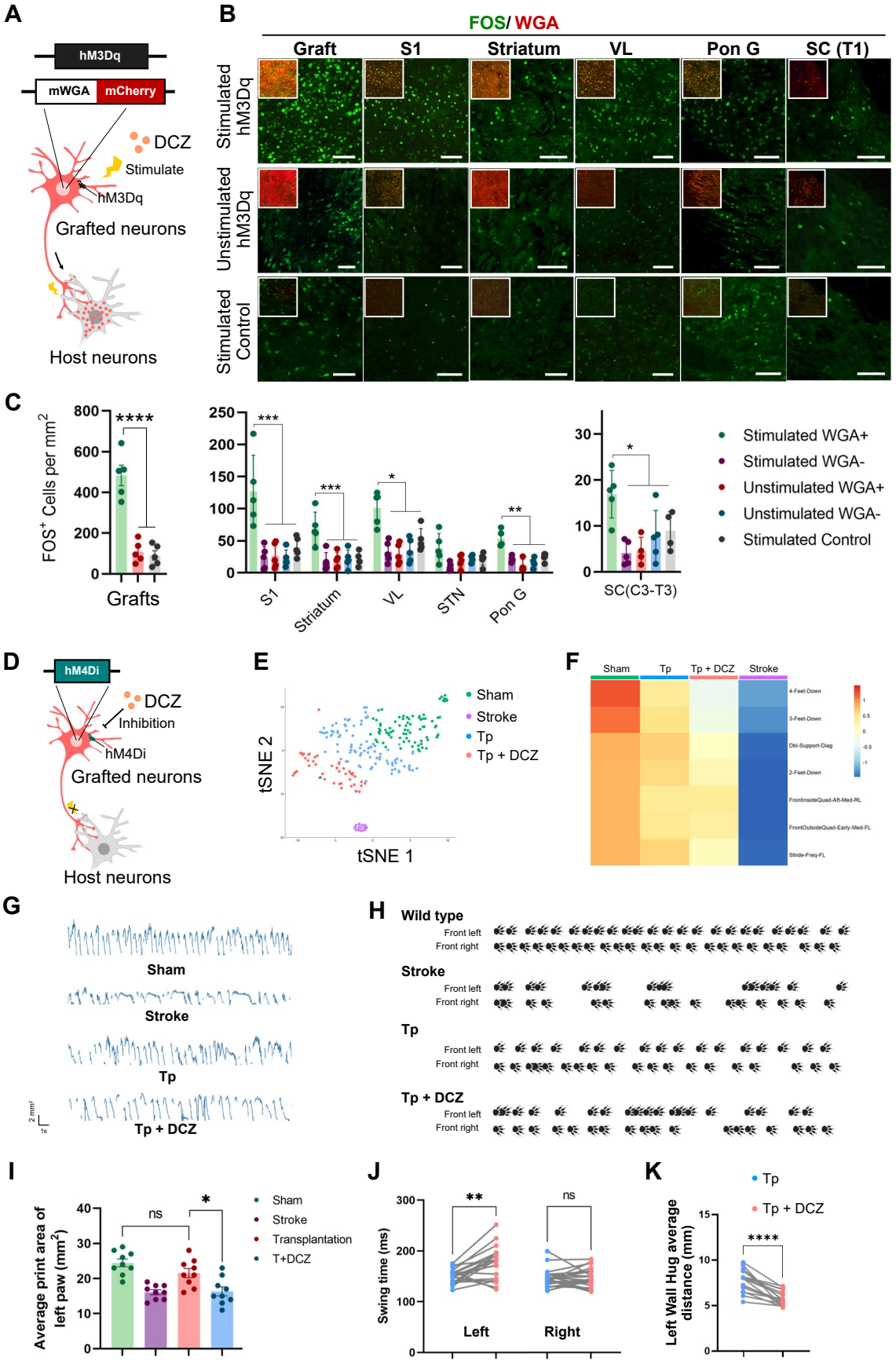

Figure 3. Transplanted cortical neurons make functional connections with host neurons.

(A) Cartoon outlining the strategy to test the functional connections between the hESC-derived neurons and host neurons by activating the grafted DREADD/ mWmC-human neurons with DCZ and examining the FOS expression in (WGA+) synaptically connected mouse neurons.

(B) Immunostaining for FOS and WGA showing the expression of FOS in WGA^+ neurons in the presence (top) or absence (middle) of DCZ at 12-month after transplantation. The bottom panels showing tissues from the animals grafted with hESC-derived neurons (without DREADD) following DCZ treatment (stimulated control). Scale bars, 100μm.

(C) Quantification of FOS-expressing cells in the grafts (left), host brain (middle) and spinal cord (right) in stroke mice, stimulated or non-stimulated. *$p<0.05$, **$p<0.01$, ***$p< 0.005$, ****$p<0.001$, two-way ANOVA test.

(D) Schematic showing the strategy to test the functional connections by inhibitory DREADD (hM4Di) hESC-derived neurons at 12-month after transplantation.

(E) tSNE visualization of clustering of gait analysis for sham, stroke, transplanted (Tp), and hM4Di activated (Tp+DCZ) mice.

(F) Heatmap showing difference in parameters among the sham, stroke, transplanted, and transplanted with hM4Di activation group from the stroke group.

(G) Traces of the front left paws touching the treadmill belt in sham, stroke, Tp, and Tp+DCZ groups.

(H) Footprints of the front paw captured in sham, stroke, Tp, and Tp+DCZ mice.

(I) Quantification of average print area of the contralateral front paw in the four groups. n=9 mice in each condition. *$p=0.0253$, two-sided Student's t-test.

(J) Quantification of swing time of the left and right front paw before and after DCZ treatment in the transplanted mice. **$p=0.0031$, paired two-sided Student's t-test.

(K) Quantification of the average distance of left wall hug before and after hM4Di activation in the transplanted mice. ****$p=0.0002$, paired two-sided Student's t-test. All Data are presented as mean±SEM.

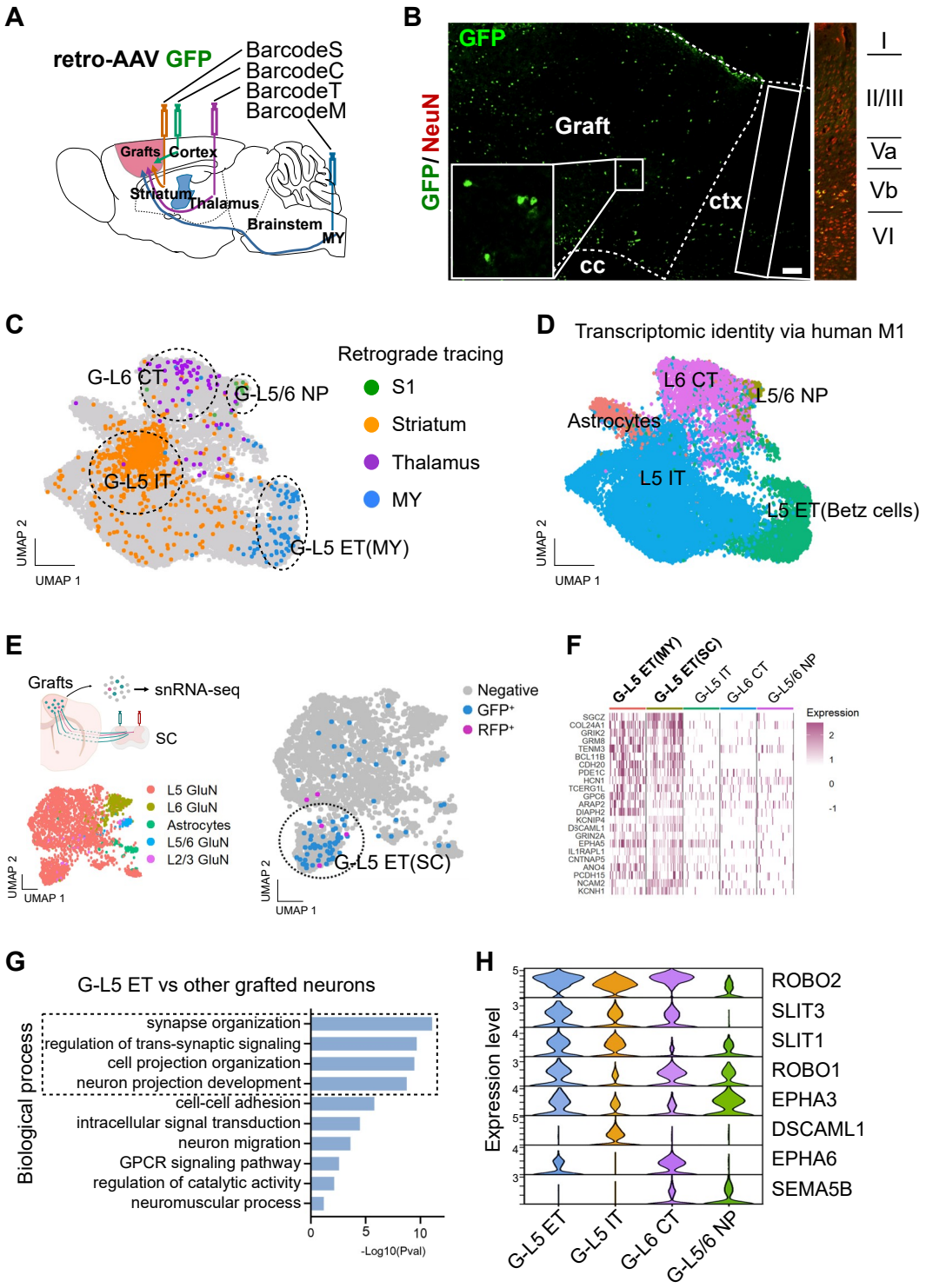

Figure 4. Transplanted cortical neuronal subtypes project to specific brain regions revealed by MRT-seq.

(A) Cartoon showing the strategy for multiple barcoded retrograde tracing by injecting AAV into the somatosensory cortex, striatum, thalamus, and medulla of transplanted mice (left).

(B) Immunostaining showing GFP labelling in the grafts and the neighboring host cortex. The inset is magnified on the right showing NeuN and GFP-labeled cells in a layered structure. Scale bars, 100μm.

(C) UMAP visualization of clustering of retro-AAV labeled nuclei in the grafts in (A).
(D) UMAP visualization showing the subtypes of transplanted cells using the human M1 snRNA-seq reference dataset. L5 ET, layer V extratelencephalic neurons; L5 IT, layer V intratelencephalic neurons; L6 CT, layer VI corticothalamic neurons; L5/6 NP; layer V/VI near-projecting neurons.
(E) UMAP visualization of grafted neurons retrogradely labelled from the SC. The experimental strategy and UMAP visualization of transplanted neuronal subtypes are shown in the left panel. UMAP visualization of transplanted neurons labelled with retro-AAV is presented in the right panel. GluN, glutamatergic neurons; Astrocytes, astrocyte lineage cells; L2/3, layer II or III; L5, layer V; L6, layer VI; L5/6, layer V or VI.
(F) Heatmap showing the top L5 ET marker expression of 50 randomly selected nuclei in each subtype of transplanted neurons.
(G) Bar plot of enriched Gene Oncology (biology process) terms of G-L5 ET (MY) in the graft dataset (C). (H) Violin plot of canonical axon guidance genes for each subtype of transplanted cortical neurons in (C). S1, primary somatosensory cortex. MY, medulla. SC, spinal cord.

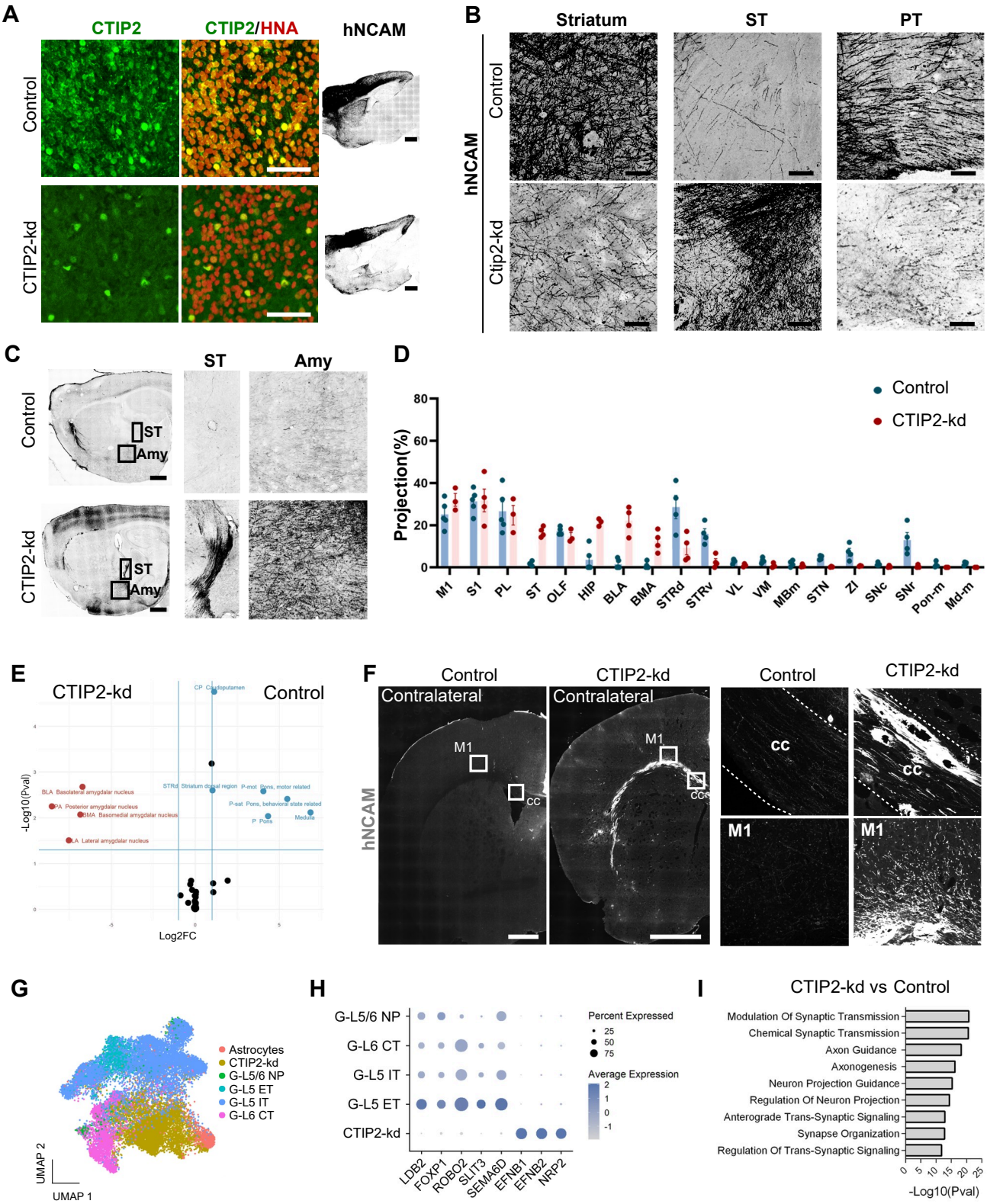

Figure 5. Grafted human cortical neurons alter the projection pattern when CTIP2 is knocked down

(A) Immunostaining for CTIP2 and HNA showing that reduction of CTIP2 expression in CTIP2-kd (bottom) than the wild-type (top) graft. Scale bars, 100μm. Right panels showing the hNCAM immunostaining on sagittal brain slices. Scale bars, 1mm.

(B) Immunostaining for hNCAM showing graft-derived axons of control cell line (top) and Ctip2-kd cell line (bottom) in the striatum, ST, and PT in the ipsilateral hemisphere of stroke mice.
(C) Immunostaining for hNCAM on the sagittal brain slices showing axon projection of the transplanted neurons derived from the control cell line (left) and CTIP2-kd cell line (right) in the stria terminalis (ST) and amygdala (Amy).
(D) Quantification of axon projection of grafted neurons in ipsilateral brain regions. n=4-5 mice in each group.
(E) Scatter plot showing brain regions with axon projection by the control cell and CTIP2-kd cell line. X: log2 fold change of axon projection, Y: -log10(p-value).
(F) Immunostaining for hNCAM on the coronal sections showing axon projection of transplanted neurons derived from the control and CTIP2-kd cell line. Right panels showed the magnification in the cc, M1. Scale bars, 1mm.
(G) UMAP visualization showing the subtypes of transplanted cells derived from control and CTIP2-kd cell lines after Seurat integration.
(H) Dot plot of top marker genes of control and CTIP2-kd neurons showing the different expression levels of axon guidance genes.
(I) Bar plot of enriched Gene Oncology – Biology Process terms between CTIP2-kd neurons versus control neurons.
All Data are represented as mean±SEM

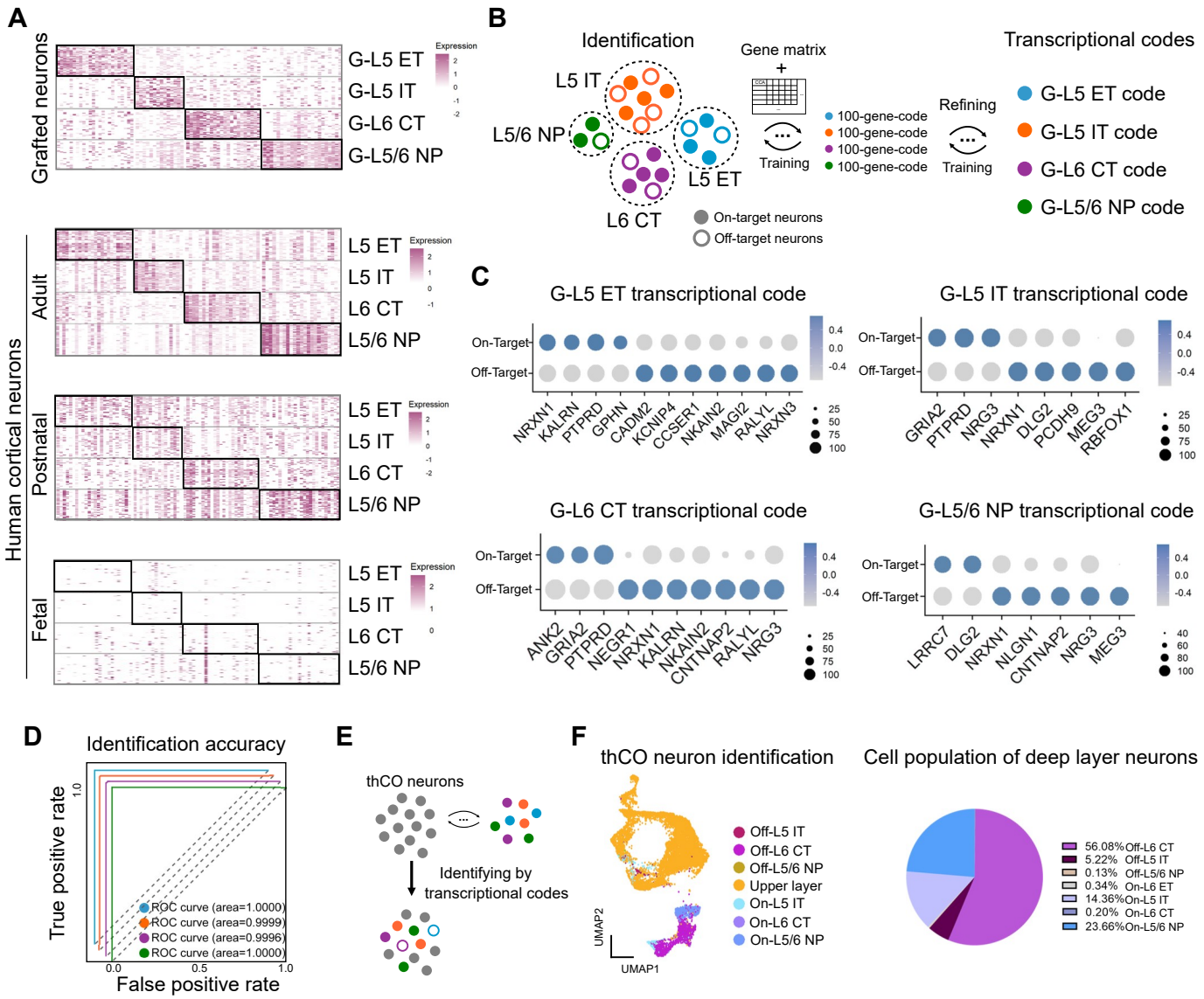

Figure 6. Transcriptional codes for grafted cortical neurons.

(A) Heatmap showing the top marker expression in 50 randomly selected nuclei in each subtype of transplanted, adult, postnatal (8-month), fetal (6-month) human cortical neurons.

(B) Schematic showing the identification of transcriptional codes with machine learning for grafted neurons.

(C) Dot plot showing the expression levels of the minimal number of genes (transcriptional codes) to identify on-target grafted neurons in four subtypes.

(D) ROC curves showing the identification accuracy of grafted neurons in each subtype.

(E) Strategy for identification of cortical neurons from transplanted human cortical organoid (thCO).

(F) UMAP visualization (left panel) and quantification (right panel) of publicly available data of transplanted cortical neurons identified by transcriptional codes. On-, On-target grafted neurons. Off-, Off-target grafted neurons.

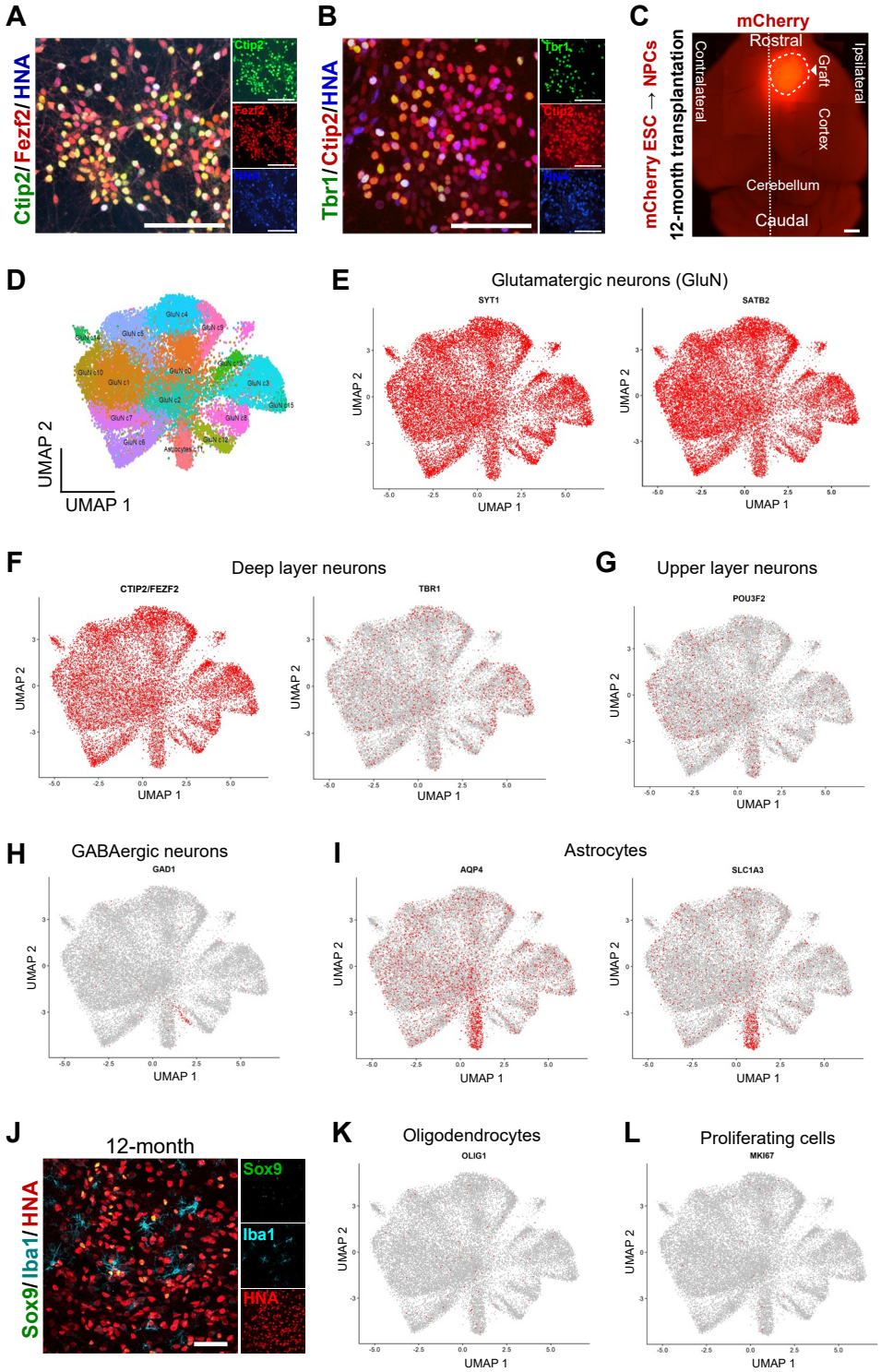

Figure S1. Characterization of human cortical neurons before and after transplantation.

(A) Immunostaining shows co-expression of CTIP2 and FEZF2 in human cortical neurons prior to transplantation. Scale bars, 200μm.

(B) Immunostaining for HNA, CTIP2, and TBR1 shows expression of deep layer marks in human cortical NPCs before transplantation. Scale bars, 200μm.

(C) Whole-mount fluorescence image shows that the graft (mCherry+) filled the ischemic motor cortex at 12 months post transplantation. Scale bars, 1mm.

(D) UMAP visualization of clustering of nuclei from grafted cells.

(E) Feature plot showing glutamatergic neuron markers SYT1+ (left) and SATB2+ (right) nuclei from (D).

(F) Feature plot showing deep layer neuron markers CTIP2+/FEZF2+ (left) and TBR1+ (right) cells.

(G) Feature plot showing upper layer neuron marker POU3F2+ cells.

(H) Feature plot showing GABAergic neuron marker GAD1+ cells.

(I) Feature plot showing astrocyte markers AQP4+ (left) and SLC1A3+ (right).

(J) Immunostaining for HNA, SOX9, and Iba1 on the brain slices showing astrocytes and microglia in the grafts at 12 months post transplantation. Scale bars, 200μm.

(K) Feature plot showing oligodendrocyte marker OLIG1 cells.

(L) Feature plot showing proliferating cell marker KI67.

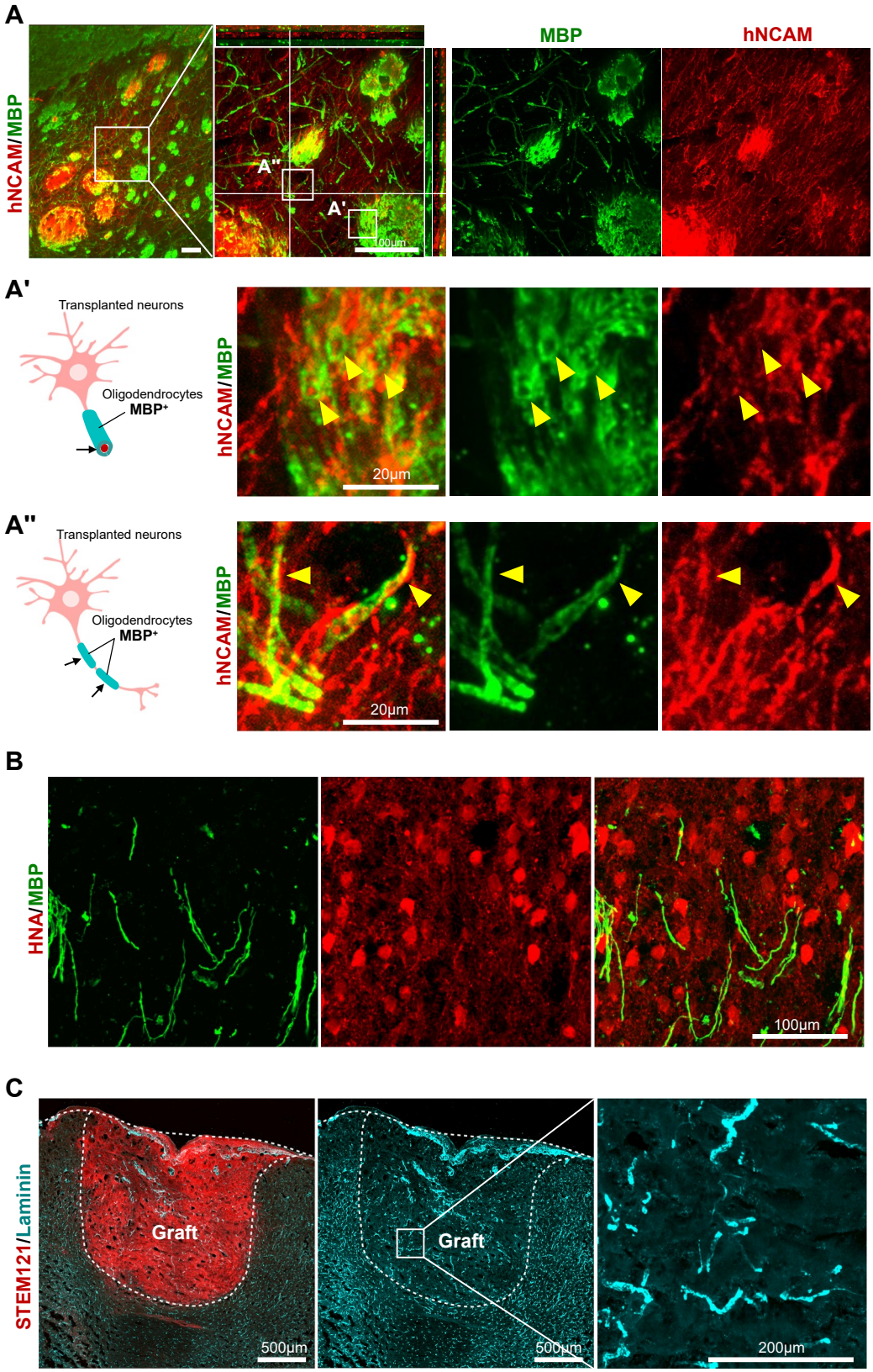

Figure S2. Myelination and vascularization in the graft.

(A) Immunostaining of hNCAM and oligodendrocyte marker MBP showing graft-derived axons are surrounded by mouse oligodendrocytes. The cross-sectional view is shown in panel (A'), and side view in panel (A''). Yellow arrowheads indicating the relationship between MBP and hNCAM signals. Scale bars, 100μm.

(B) Immunostaining with MBP (oligodendrocyte marker) and HNA showing no expression of MBP in transplanted cells. Scale bars, 100μm.

(C) Immunostaining with STEM121 and endothelial marker Laminin on the brain slices of 12-month after transplantation, showing the mouse blood vessel endothelium grew into the graft. Scale bars, 500μm. 200μm in magnification.

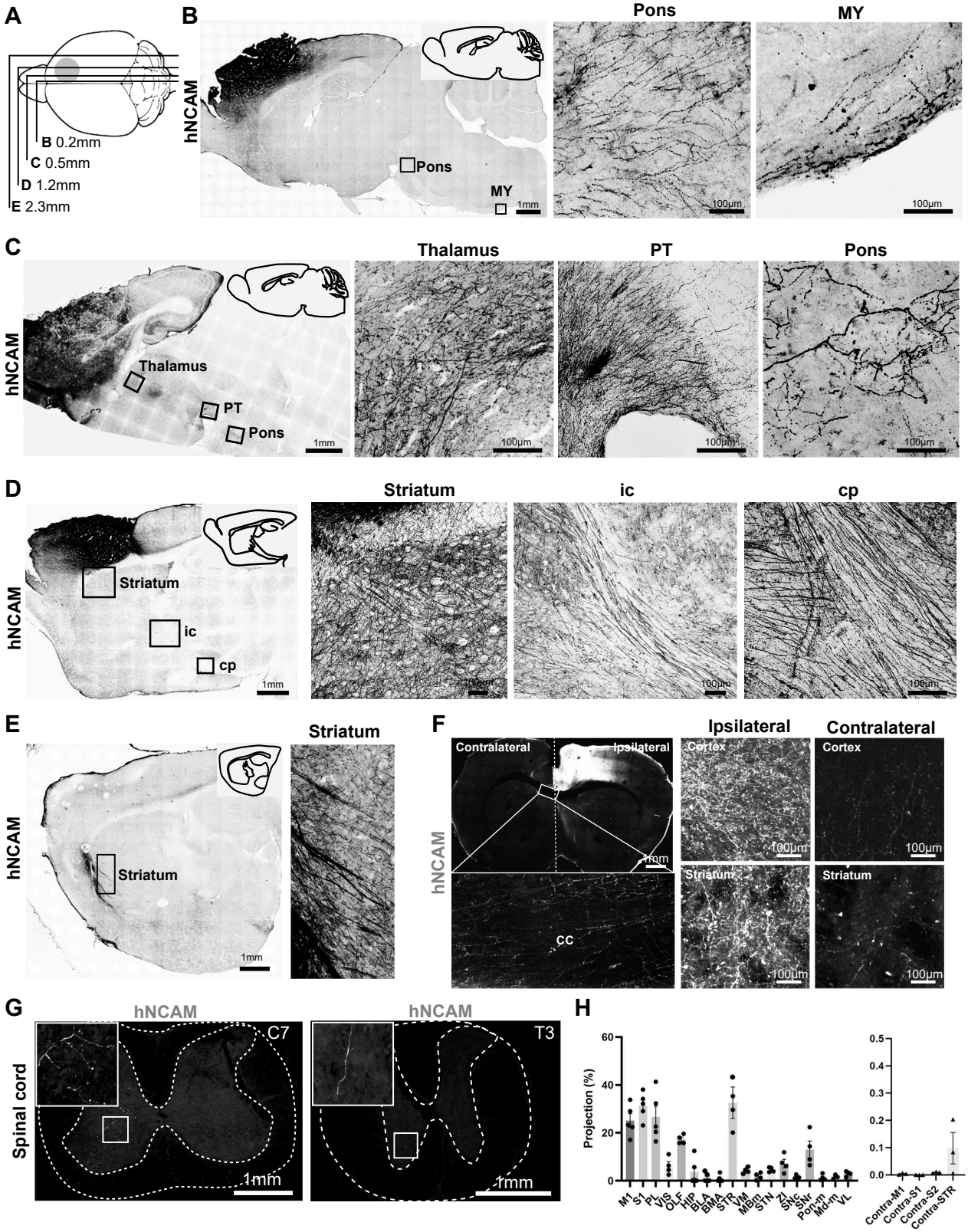

Figure S3. Transplanted human cortical neurons rebuild the motor-related neural circuits.

(A) Schematic diagram showing the planes for brain sections.

(B to E) Immunostaining of hNCAM showing axon projections by the grafted neurons in Pons and MY (B), thalamus, PT and Pons (C), striatum, ic and cp (D), and S1 and striatum (E), in stroke mice 12 months post transplantation. Scale bars, 1mm. 100μm in magnification.

(F) Immunostaining for hNCAM showing axon projections by the grafted neurons in the contralateral and ipsilateral hemispheres at 12 months after transplantation. Scale bars, 1mm. 100μm in the magnification.
(G) Immunostaining for hNCAM showing graft-derived axons in the contralateral spinal cord C7 (top) and T3 (bottom) at 12 months after transplantation. Scale bars, 1mm.
(H) Quantification of axon projection of grafted neurons in brain regions.
All Data are presented as mean±SEM.

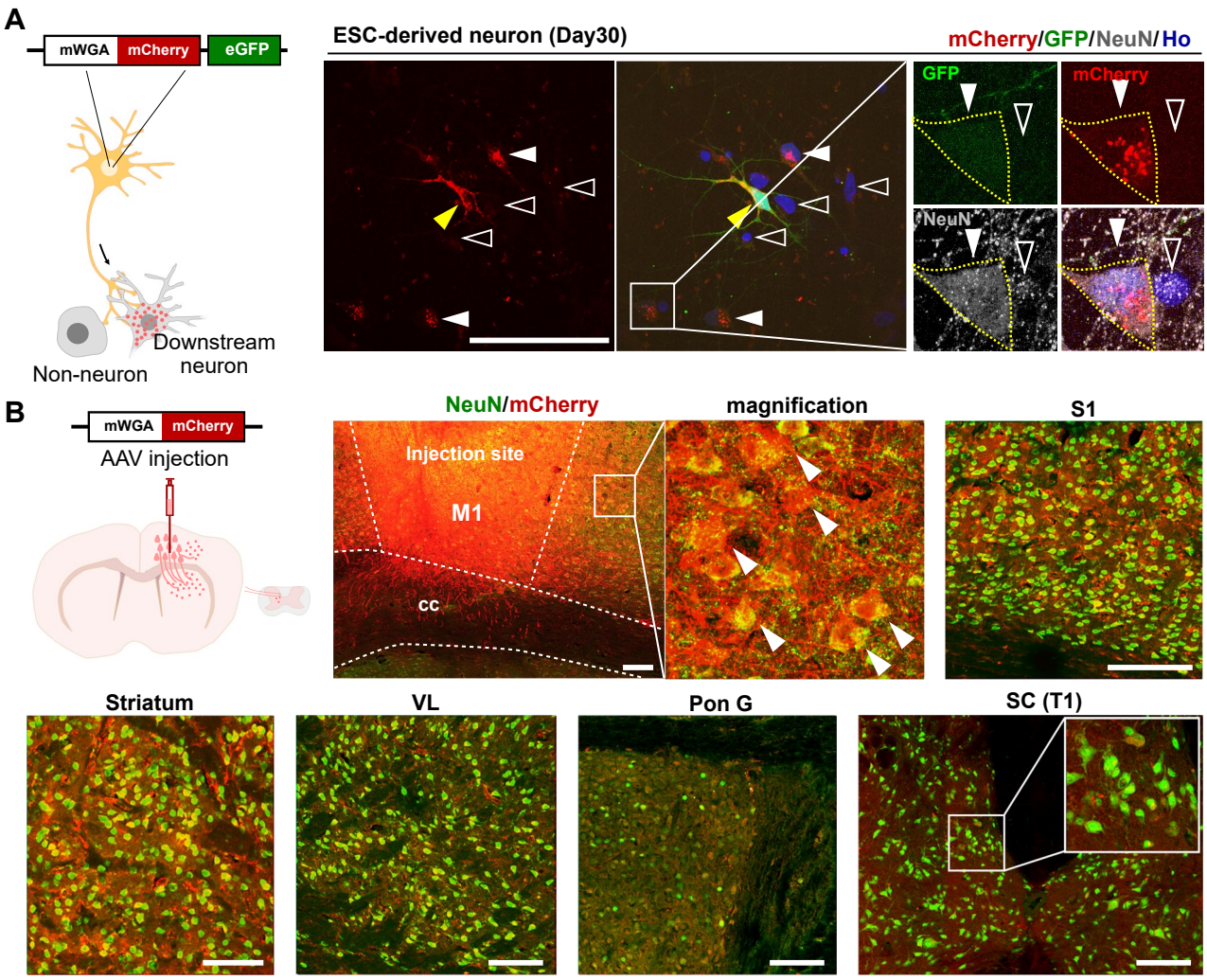

Figure S4. Anterograde trans-synaptic tracer mWmC.

(A) Strategy for generation of the mWmC-eGFP cell line (left). Immunostaining showing expression of GFP and mCherry(mWmC) in 2D-cultured neurons 30 days of differentiation (right). Scale bars, 100μm.

(B) Strategy for injection of mWmC-AAV in M1c of the mouse brain. Immunostaining showing mCherry (mWmC) detection in the S1,striatum, VL, Pon G and T1 (spinal cord) in the mouse CNS. Scale bars, 200μm.

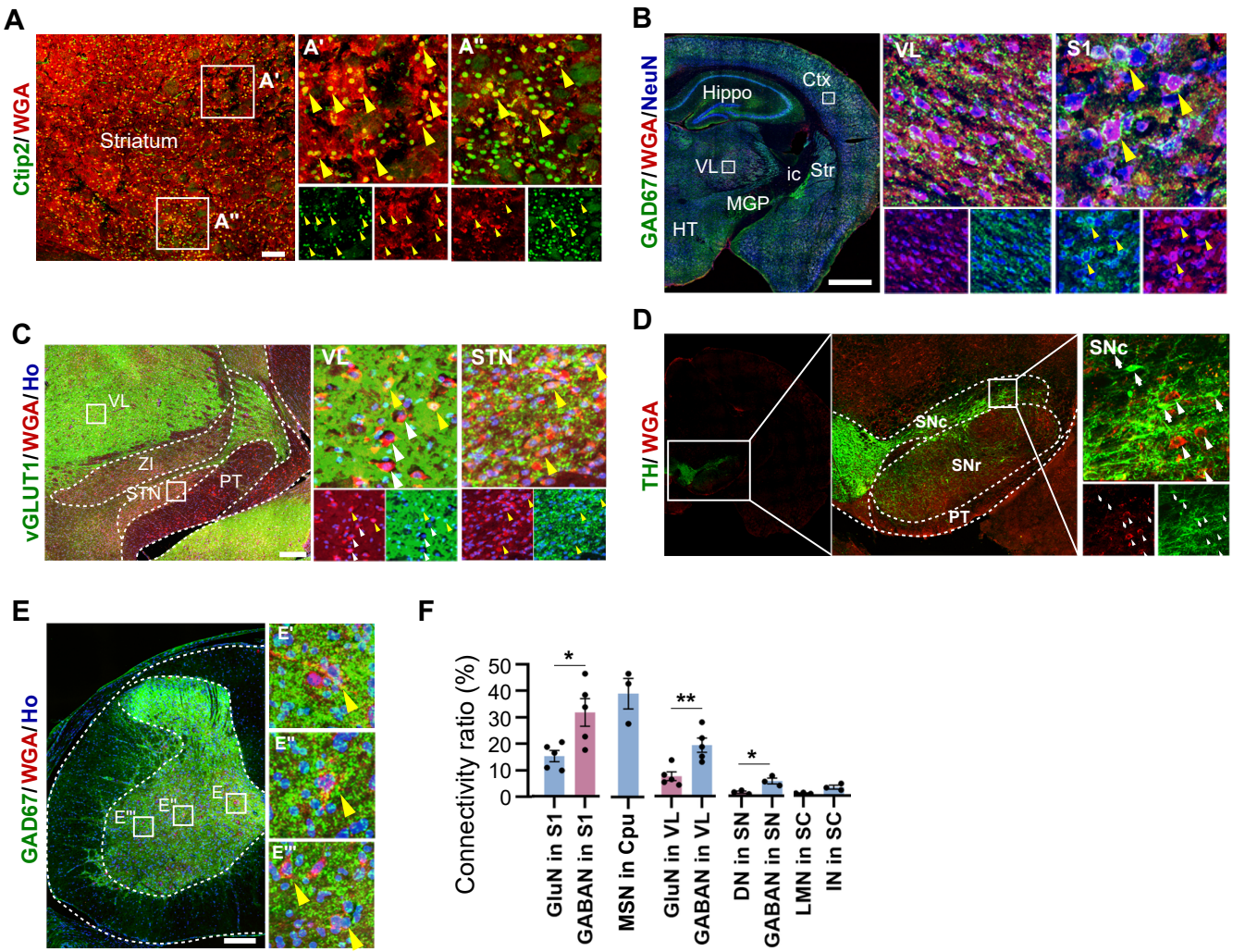

Figure S5. Transplanted neurons synapse with specific target neurons.

(A) Immunostaining for WGA and Ctip2 showing that host medium spiny neurons (Ctip2$^+$) were labelled by WGA in the striatum at 12-mpt. Right panels show magnified view of the insets in the dorsal (A') and ventral (A") striatum. Yellow arrowheads indicate WGA$^+$/Ctip2$^+$ neurons. Scale bars, 100μm.

(B) Immunostaining with NeuN, WGA, and GAD67 showing that GABAergic neurons in the cortex and thalamus were WGA positive. Right panels show magnification of VL and S1. Yellow arrowheads indicate WGA$^+$/GAD67$^+$/NeuN$^+$ cells. Scale bars, 1mm.

(C) Immunostaining for vGLUT1 and WGA showed that WGA labels (vGLUT1$^+$) glutamatergic neurons in the VL and STN. The magnification was shown in the right panels. Yellow arrowheads indicate WGA$^+$/vGluT1$^+$ cells. White arrowheads indicate WGA$^+$/ vGluT1$^-$cells. Scale bars, 100μm.

(D) Immunostaining showing no overlap of WGA with hostdopaminergic neurons (TH+) in the substantia nigra. White arrowheads indicate WGA+/ TH- cells. White arrows indicate TH+/WGA- cells. Scale bars, 100μm.

(E) Immunostaining showing GAD67-expressing WGA-labeled host neurons in the spinal cord. The insets are magnified on the right, yellow arrowheads indicate WGA$^+$/ GAD67$^+$ cells. Scale bars, 100μm.

(F) Quantification of the ratio of host neurons receiving output connections of grafted cells in different brain regions. *$p<0.05$, **$p<0.01$, two-sided Student's t-test. Data are presented as mean±SEM.

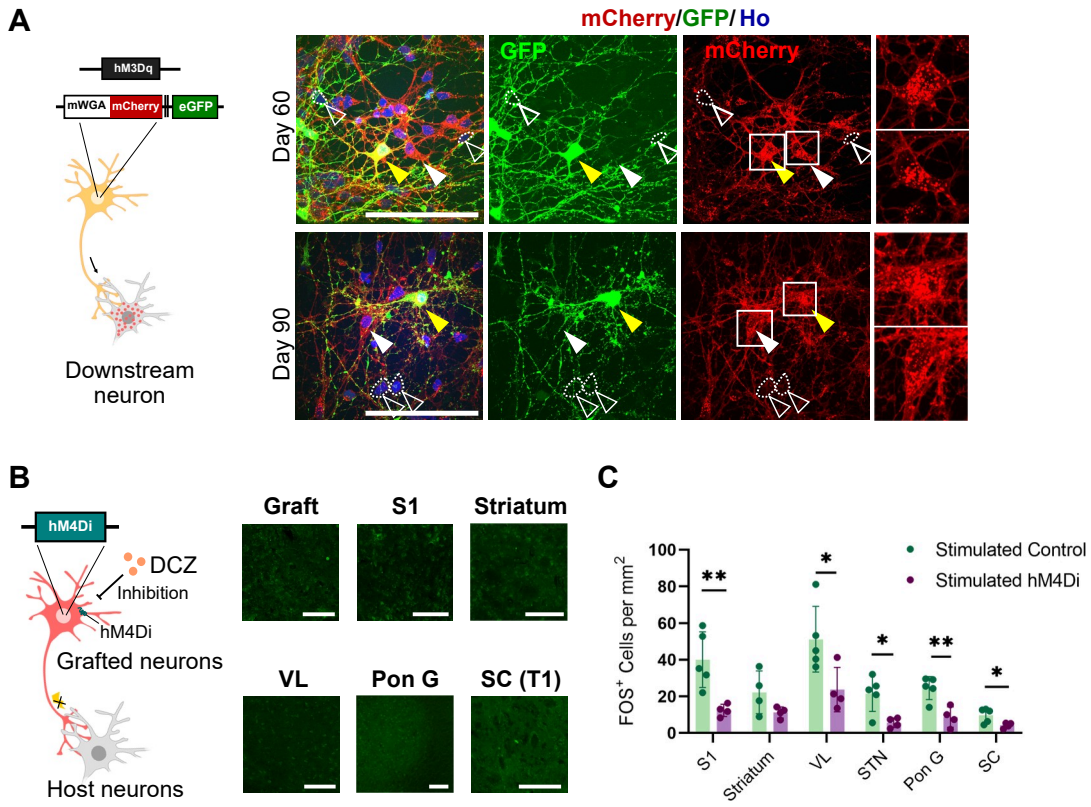

Figure S6. DREADD/mWmC ESC-derived neurons.

(A) Strategy for generation of hM3Dq-mCherry–mWmC-eGFP cell line (left). Immunostaining showing expression of GFP and mCherry(mWmC) in 2D-cultured neurons 60 (right top) and 90 (right bottom) days of induction. Scale bars, 100μm.

(B) Immunostaining for FOS showing the expression of FOS in host neurons in the presence of DCZ at 12-month after hM4Di neural transplantation. The left panel showing hM4Di neurons following DCZ treatment (inhibited neurons). Scale bars, 200μm.

(C) Quantification of FOS-expressing cells in the host brain and spinal cord in stroke mice. *$p<0.05$, **$p<0.01$, Student's t-test.

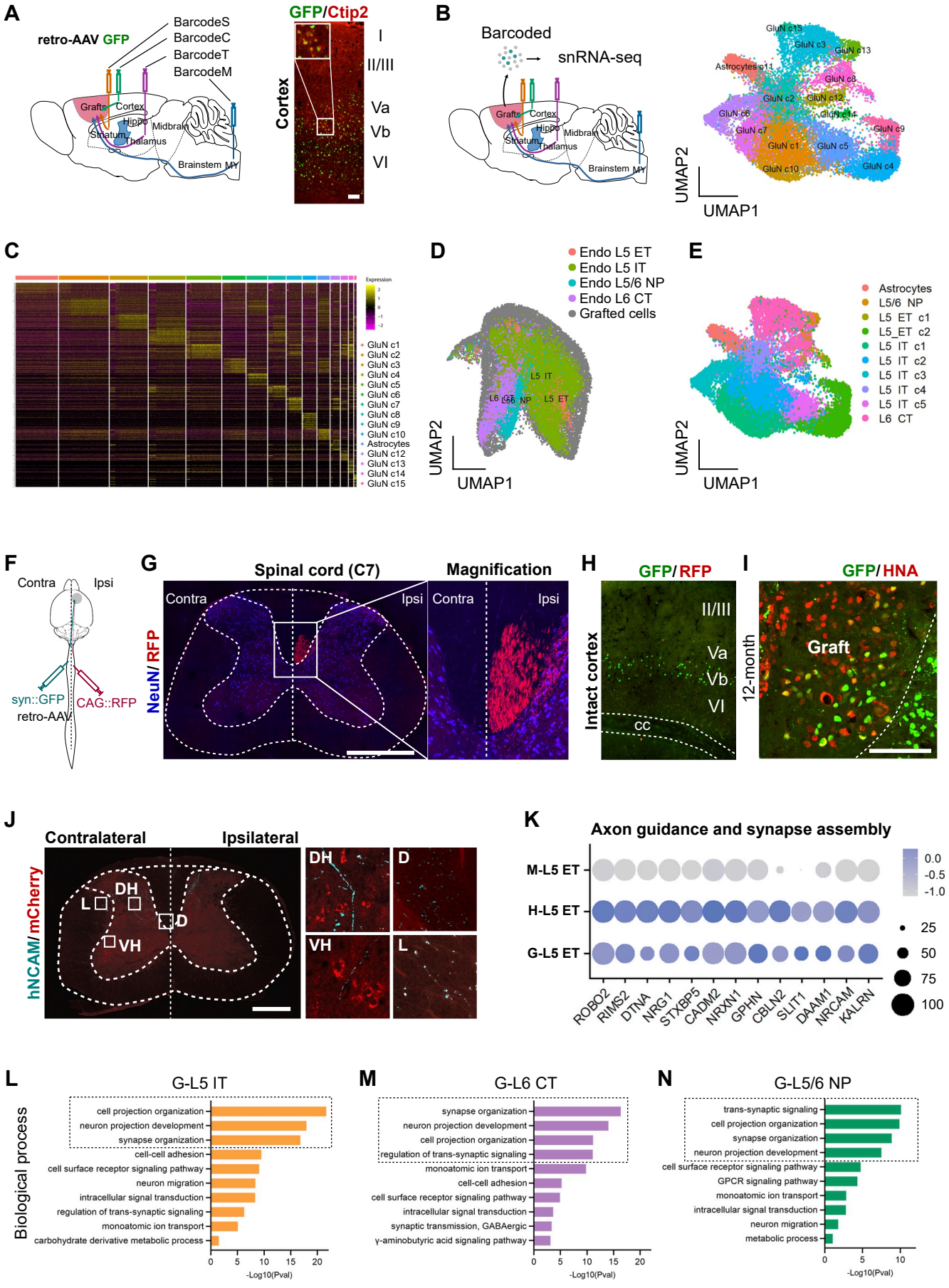

Figure S7. Retrograde tracing for transplanted neurons.

(A) Strategy for injection of retrograde-AAV GFP with barcodes in the transplanted mouse brain (left). Immunostaining for GFP and Ctip2 showing retrograde-AAV labelled layer V neurons in the intact cortex (right). Scale bars, 200μm.
(B) Strategy for MRT-seq at 5 weeks after AAV injection. UMAP showing clusters of nuclei from transplanted cells extracted from the mouse brain with barcoded retro-AAV-GFP injection.
(C) Heatmap showing marker expression of clusters in (B).
(D) UMAP showing the grafted cells and human M1c snRNA-seq reference dataset after Seurat integration.
(E) UMAP showing clustering of nuclei from grafted cells using label transferred from the human M1c snRNA-seq reference dataset.
(F) Strategy for retrograde AAV injection in the spinal cord of transplanted stroke mice at 12 months after transplantation.
(G) Immunostaining for RFP and NeuN showing retrograde AAV-RFP-labelled axons in the ipsilateral spinal cord of transplanted stroke mice. Scale bars, 1mm.
(H) Immunostaining of retrograde-AAV-GFP and RFP-labeled neurons in the cortex of stroke mice. Scale bars, 200μm.
(I) Immunostaining for GFP and HNA showing the transplanted neurons were labelled by retro-AAV. Scale bars, 200μm.
(J) Immunostaining showing axonal projection (hNCAM+) and output connection (mCherry+) of grafted cells to the spinal cord (C8). DH, dorsal horn. D, dorsal funiculus. VH, ventral horn. L, lateral funiculus. Scale bars, 500μm.
(K) Dot plot of top axon guidance/synapse assembly genes of human L5 ET versus mouse L5 ET neurons. The genes expression on Grafted L5 ET neurons is represented at the bottom of the plot for top feature genes.
(L-N) Bar plot of enriched Gene Oncology – Biology Process terms of cluster G-L5 IT (L), G-L6 CT (M), and G-L5/6 NP (N) in the graft dataset.

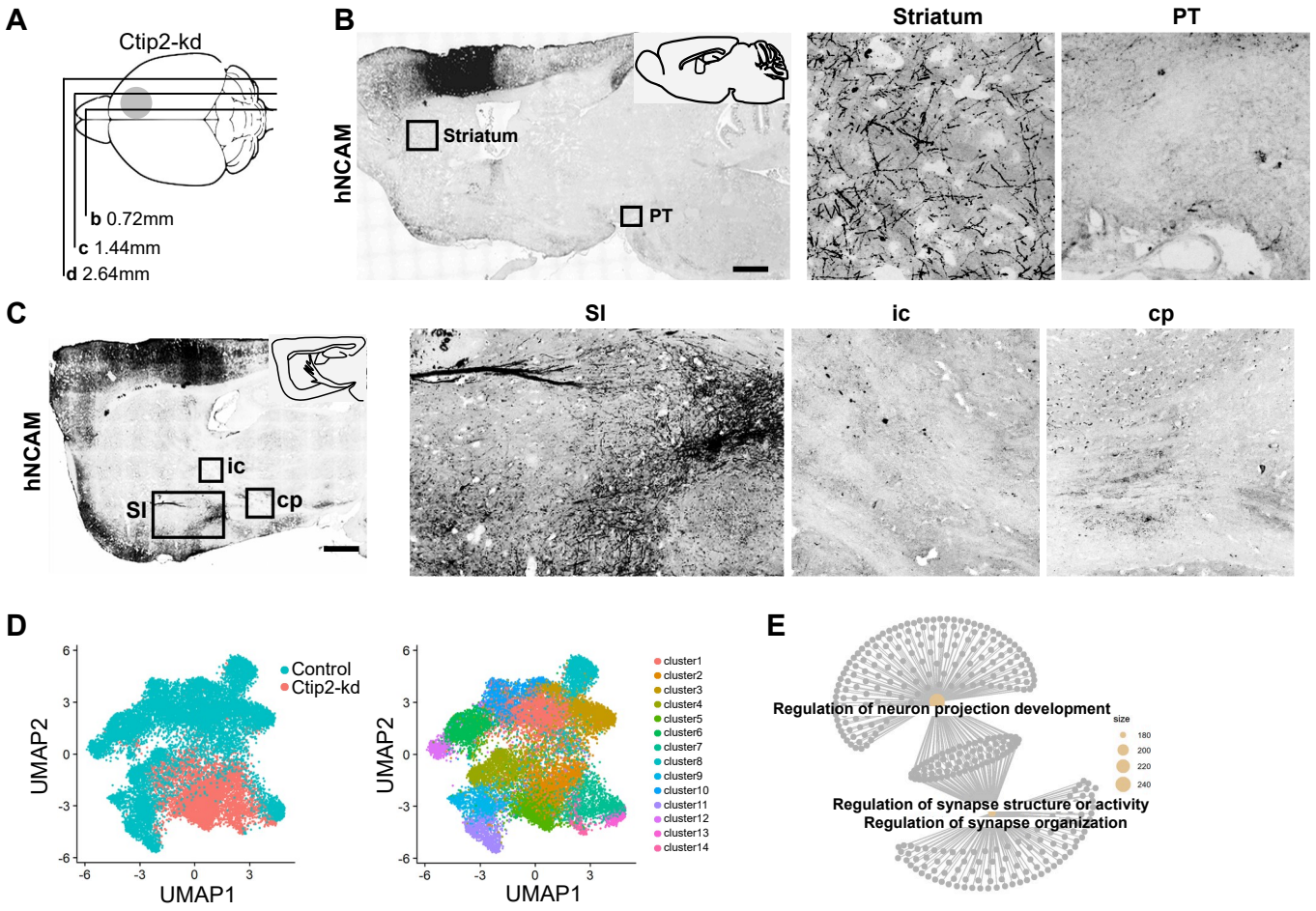

Figure S8. The projection pattern of transplanted CTIP2-kd neurons

(A) Schematic for brain sections of mice transplanted with CTIP2-kd human neurons.

(B-C) Immunostaining of hNCAM showing axon projections by the grafted CTIP2-kd neurons in the striatum and PT (B), SI, ic and cp (C) at 12 months post transplantation. Scale bars, 1mm.

(D) UMAP visualization showing the subtypes of transplanted cells derived from control and CTIP2-kd cell lines after Seurat integration.

(E) Network of enriched Gene Oncology – Biology Process terms of cluster CTIP2-kd neurons versus control neurons.

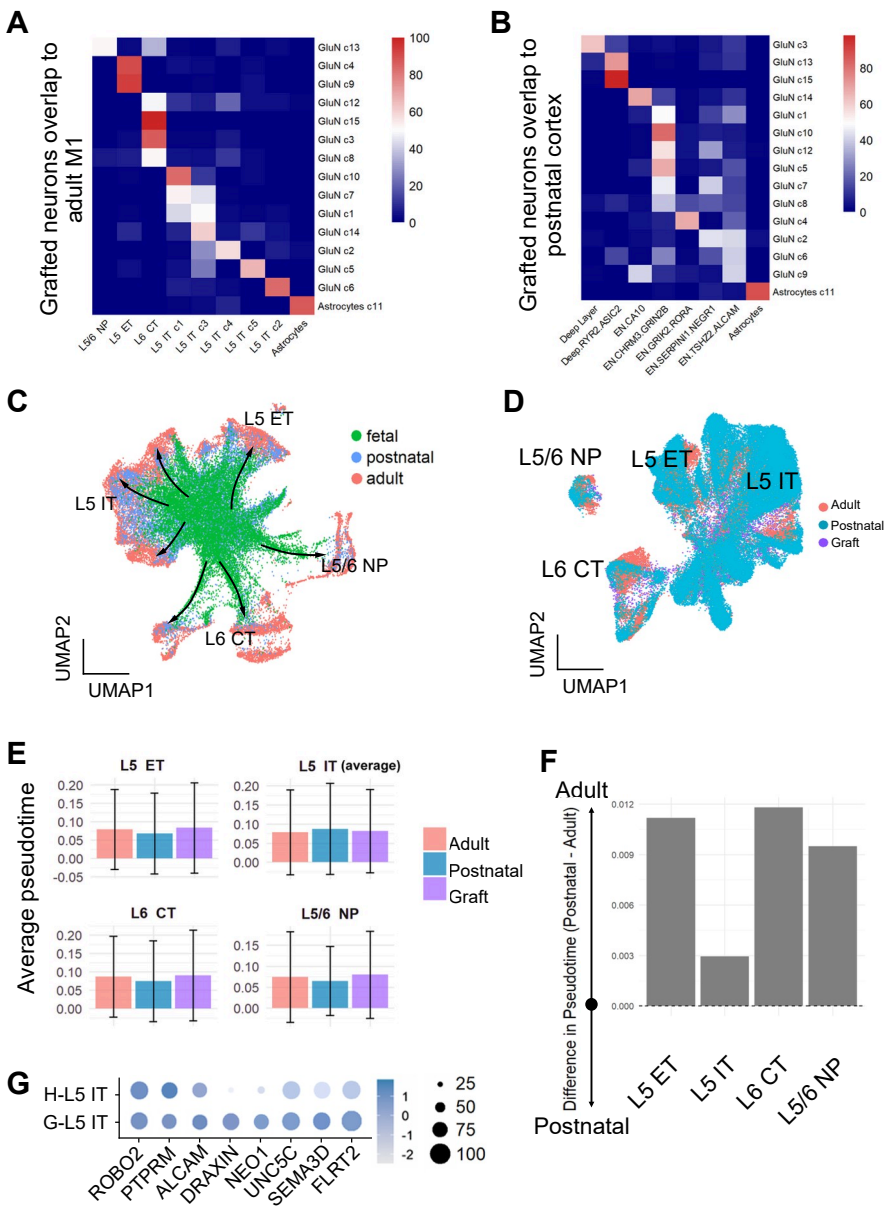

Figure S9. Comparison of transplanted neurons with endogenous human neurons.

(A and B) Heat maps of grafted cell clusters overlap by RNA-seq integration with human adult (A) and postnatal (B) cortical cell clusters.

(C) UMAP plots showing the maturation trajectory in each subtype of human cortical neurons from fetal, postnatal, and adult cortex.

(D) UMAP plots showing the transplanted, postnatal, and adult cortical neurons after Seurat integration.

(E) Quantification of pseudotime in each subtype of cortical neurons.

(F) Bar plot showing the difference in pseudotime distance between grafted neurons and postnatal versus adult neurons, indicating their relative similarity.

(G) Dot plot of canonical guidance gene expression on G-L5 ET neurons. The genes expression on human L5 ET neurons (H-L5 ET) is represented on the top of the plot for top feature genes.